TEMPERATURE DEPENDENCE OF THE SPECTROSCOPIC AND STRUCTURAL PROPERTIES OF $TlGaS_2$ AND $TlInS_2$ CRYSTALS

A THESIS SUBMITTED TO
THE GRADUATE SCHOOL OF NATURAL AND APPLIED SCIENCES
OF
MIDDLE EAST TECHNICAL UNIVERSITY

BY

MUHAMMED AÇIKGÖZ

IN PARTIAL FULFILLMENT OF THE REQUIREMENTS

FOR

THE DEGREE OF MASTER OF SCIENCE

IN

PHYSICS

AUGUST 2004

Approval of the Graduate School Natural and Applied Sciences.

____

Prof. Dr. Canan Özgen
Director

I certify that this thesis satisfies all the requirements as a thesis for the degree of Master of Science.

____

Prof. Dr. Sinan Bilikmen
Head of Department

This is to certify that we have read this thesis and that in our opinion it is fully adequate, in scope and quality, as a thesis for the degree of Master of Science.

Prof. Dr. Nizami Hasanli Co-supervisor	Prof. Dr. Hüsnü Özkan Supervisor

Examining Committee Members

Prof. Dr. Yakup Cevdet Akgöz	(METU, ES)	
Prof. Dr. Hüsnü Özkan	(METU, PHYS)	
Prof. Dr. Nizami Hasanli	(METU, PHYS)	
Prof. Dr. Bülent Akınoğlu	(METU, PHYS)	
Assoc. Prof. Dr. Mehmet Parlak	(METU, PHYS)	

I hereby declare that all information in this document has been obtained and presented in accordance with academic rules and ethical conduct. I also declare that, as required by these rules and conduct, I have fully cited and referenced all material and results that are not original to this work.

Name, Last name: Muhammed Acikgoz

Signature :

ABSTRACT

TEMPERATURE DEPENDENCE OF THE SPECTROSCOPIC AND STRUCTURAL PROPERTIES OF $TlGaS_2$ AND $TlInS_2$ CRYSTALS

Açıkgöz, Muhammed

M. S., Department of Physics

Supervisor: Prof. Dr. Hüsnü Özkan

Co-supervisor: Prof. Dr. Nizami Hasanli

August 2004, 71 pages

The results of photoluminescence (PL) spectra of $TlGaS_2$ single crystal were reported in the 500-1400 nm wavelength and in the 15-115 K temperature range. Three broad PL bands with an asymmetric Gaussian lineshapes were observed to be centered at 568 nm (A-band), 718 nm (B-band) and 1102 nm (C-band). The shift of the emission band peak energy as well as the change of the half-width of the emission band with temperature and excitation laser intensity were also studied. We analyzed the observed results using the configurational coordinate (CC) model.

The powder diffraction patterns of $TlInS_2$ and $TlGaS_2$ crystals were obtained and the diffraction data were indexed using CRYSFIRE computer program packet. $TlInS_2$ has hexagonal system with parameters a = 3.83 and c = 14.88 A^o. $TlGaS_2$ has monoclinic system with parameters a = 9.62, b = 4.01 and c = 7.52 A^o with β= 96.30^o. Our diffraction studies at low temperatures did not reveal any phase

transition for $TlInS_2$ as reported in the literature. The specific heat capacities of both $TlInS_2$ and $TlGaS_2$ crystals calculated from Differential Scanning Calorimetry (DSC) measurements at low temperatures are reported in the thesis.

Keywords: Photoluminescence, ternary compounds, band structure, indexing, phase transition, specific heat capacity.

ÖZ

$TlGaS_2$ ve $TlInS_2$ KRİSTALLERİNİN SPEKTROSKOPİK VE YAPISAL ÖZELLİKLERİNİN SICAKLIK DEĞİŞİMLERİ

Açıkgöz, Muhammed

Yüksek Lisans, Fizik Bölümü

Tez Yöneticisi: Prof. Dr. Hüsnü Özkan

Ortak Tez Yöneticisi: Prof. Dr. Nizami Hasanli

Ağustos 2004, 71 sayfa

$TlGaS_2$ katlı kristalinin fotoışıma spektrumunun sonuçları 500-1400 nm dalga boyu diliminde ve 15-115 K sıcaklık aralığında elde edildi. Merkezleri 568 nm (A-band), 718 nm (B-band) ve 1102 nm (C-band) olan asimetrik çizgi şekilli üç tane geniş fotoışıma bandı gözlendi. Sıcaklık ve lazer uyarma yoğunluğuyla ışıma bandının tepe noktasındaki kayma aynı şekilde ışıma bandının yarı genişligindeki değişme de çalışıldı. Elde edilen sonuçlar konfigürasyon koordinat model kullanılarak analiz edildi.

$TlInS_2$ ve $TlGaS_2$ kristallerinin toz kırınım desenleri elde edildi ve kırınım dataları CRYSFIRE bilgisayar program paketi kullanılarak indekslendi. $TlInS_2$ heksagonal sisteme sahiptir ve örgü parametreleri a = 3.83 ve c = 14.88 A^o olarak belirlenmiştir. $TlGaS_2$ monoklinik sisteme sahiptir ve örgü parametreleri a = 9.62, b =4.01, c = 7.52 A^o ve β = 96.30^o olarak belirlenmiştir. $TlInS_2$ için düşük sıcaklıklardaki kırınım

çalışmalarımız literatürde rapor edilmiş olan faz geçişlerini ortaya çıkarmadı. $TlInS_2$ ve $TlGaS_2$ kristallerinin Diferansiyel Tarama Kalorimetre ölçümleri yapıldı ve düşük sıcaklıklarda ısınma ısıları hesaplandı.

Anahtar kelimeler: Fotoışıma, üçlü bileşikler, band yapısı, indeksleme, faz geçişleri, belli ısı kapasitesi.

To My Lovers...

ACKNOWLEDGMENTS

I would like to thank all who helped me to have the opportunity and possibility to continue the graduate study and to prepare this thesis.

My sincere gratitude and deep appreciation go to Prof. Dr. Hüsnü Özkan and Prof. Dr. Nizami Hasanli for their kind and supervision during this study.

At the same time, I am also grateful to Prof. Dr. Atilla Aydınlı for his guidance and laboratory opportunity at Bilkent University.

I am grateful to all staff of Superconductivity laboratory of METU, Characterization laboratory of ANAEM and Advanced Physics laboratory of Bilkent University.

TABLE OF CONTENTS

PLAGIARISM……………………………………………………………….…iii

ABSTRACT………………………………………………………………......iv

ÖZ………………………………………………………………………….....vi

DEDICATION……………………………………………………………...viii

ACKNOWLEDGMENTS…………………………………………………...ix

TABLE OF CONTENTS…………………………………………………..…x

LIST OF FIGURES………………………………………………………....xii

LIST OF TABLES…………………………………………………………..…xiv

CHAPTER

1 INTRODUCTION…………………………………………………….…1

2 THEORETICAL CONSIDERATIONS…………………………….…6

2.1 Introduction……………………………………………………...6

2.2 Electronic Properties of Semiconductors………………………..6

2.2.1 Band Structure ……………………………………….....7

2.2.2 Impurity States……………………………………………….7

2.2.3 Holes in Semiconductors…………………………….…8

2.2.4 Extrinsic and Intrinsic Semiconductors……………………..9

2.2.5 Defects……………………………………………….....10

2.3 Optical Properties of Semiconductors…………………….....11

2.3.1 Luminescence…………………………………………....11

2.3.2 Photoluminescence…………………………………………....12

2.3.3 Recombination Mechanisms………………………………..14

2.3.3.a Band-to-band Transition…………………………...….16

2.3.3.b Free-to-bound Transition……………………………..….17

2.3.3.c Donor Acceptor Pair Transition……………………….…18

2.3.3.d Excitons and Bound Exciton Emission……………….….19

2.3.4 Excitation Power Dependence of PL in Semiconductor....…20

2.4 Indexing of Powder X-ray Diffraction (XRD) Pattern…………...24

2.5 Diffraction Scanning Calorimetry……...……………………...….28

2.5.1 Heat Capacity Determination using DSC…………………..30

3 RESULTS AND DISCUSSION…………………………………………...33

3.1 Introduction……………………………………………………......33

3.2 PL Spectra Analysis……………………………………….……...33

3.2.1 Experimental Details………………………………………...33

3.2.2 Results and Discussion……………………………….……..34

3.3 Results of XRD Measurements………………………………..…49

3.4 Temperature-dependent XRD Measurements…………………....55

3.5 Results of DSC Measurements…………………………………...59

4 CONCLUSIONS…………………………………………………………….…66

REFERENCES……………………………………………………………………...68

LIST OF FIGURES

2.1 Excitation and recombination transitions……………………………………..…....16

2.2 DSC setup used in experiments……………………………………………..…30

2.3 A basic figure of heat flow versus temperature plot…………………………...31

3.1 PL setup used in experiments………………………………………………….35

3.2 PL spectrum of $TlGaS_2$ crystal in the 500-1200 nm wavelength range at T = 15 K. Excitation laser intensity L = 19.49 W cm^{-2}……………………......36

3.3 PL spectra of $TlGaS_2$ crystal in the 15-40 K temperature range and 1000-1250 nm wavelength region. Excitation laser intensity L = 19.49 Wcm^{-2}…………………..…………………………………………......39

3.4 PL spectra of $TlGaS_2$ crystal in the 15-115 K temperature range and 1000-1250 nm wavelength region. Excitation laser intensity L = 19.49 W cm^{-2} ………………………………………………………………...40

3.5 Temperature dependence of integrated PL band intensity for $TlGaS_2$ crystal. The arrow at T = 60 K shows the starting point of the intensive quenching process. (a) are the experimental data, (b) gives the theoretical fit using equation (3.1), (c) is only the guide for eye…………………………………....41

3.6 Pl spectra of $TlGaS_2$ crystal as a function of excitation laser intensity at T= 15 K………………………………………………………………………...43

3.7 Dependence of integrated PL band intensity on excitation laser intensity at T = 15 K. The solid curve gives the theoretical fit using equation (3.2)……....44

3.8 Temperature dependence of the emission band peak energy for $TlGaS_2$ crystal. The dotted line is only guide for the eye...…………….……..46

3.9 Variation of the half-width with square root of temperature for $TlGaS_2$ crystal emission band. The solid curve is a plot of equation (3.4) with $h\nu_e$ = 0.011 eV……………………………………………………………………47

3.10 Band model (a) and configurational coordinate (CC) model (b) of $TlGaS_2$ crystal at T = 15 K…………………………………………………………….48

3.11 X-ray Powder Diffraction Pattern of $TlInS_2$…………………………………..52

3.12 X-ray powder diffraction pattern of $TLGaS_2$……………………………..…..53

3.13 Fragments of diffraction patterns of the $TlInS_2$ crystal at various sample temperatures T, K: 215, 213, and 200, from top to down…………………….....56

3.14 Fragments of diffraction patterns of the $TlInS_2$ crystal at various sample temperatures T, K: 200, 195, and 193, from top to down…………………….....57

3.15 Fragments of diffraction patterns of the $TlInS_2$ crystal at two sample temperatures T, K: 250, and 83, from top to down……………..…………….....58

3.16 DSC curves of 1-baseline, 2-$TlInS_2$, and 3-$TlGaS_2$………………………......62

3.17 Temperature dependence of the specific heat of a $TlGaS_2$ single crystal determined in the range 170-240 K……………………………………………..63

3.18 Temperature dependence of the specific heat of a $TlInS_2$ single crystal determined in the range 170-280 K……………………………………………..64

LIST OF TABLES

3.1 The TREOR90 outputs from the X-ray diffraction measurements of $TlGaS_2$……………………………………………………………….54

3.2 Calculated heat capacities of $TlInS_2$ and $TlGaS_2$ at various temperatures...65

CHAPTER 1

INTRODUCTION

All the materials can be classified into three main groups in terms of their electrical properties: conductors, semiconductors and insulators. A useful way to visualize the difference between conductors, insulators, and semiconductors is to plot the available energy states for electrons in the materials. Instead of having discrete energies as in the case of free atoms, in solids the available energy states form bands. Crucial to the conduction process is whether or not there are electrons in the conduction band. In conductors like metals, the valence band overlaps the conduction band. In insulators, the electrons in the valence band are separated by a large gap from the conduction band. In semiconductors, there is a small enough gap between the valence and conduction bands that thermal or other excitations can bridge the gap.

The study of semiconductors started in the 1870s, when W. Smith discovered the selenium photoconductivity that followed the first attempts to use selenium in the devices for the visual image transport by telegraph [1].

In the previous decades researchers discovered many types of binary and ternary semiconductors. They investigated various parameters, such as mobility, defect mechanism, impurities and carrier transport, related to their features and applications in the technology.

Photoluminescence (PL) spectroscopy is one of the most important techniques which is very suitable and widely used. The first truly scientific investigation of PL

was carried out by Sir George Gabriel Stokes in 1852. His famous paper "On the charge of Refrengibility of light "[2] still makes excellent reading for its masterly style. Stokes coined the word fluorescence "from flour-spar, as the analogous term brightness is derived from the name of a mineral." This term is still used, although in a light sense. Luminescence stimulated by non-ionizing optical radiation, more properly, is called photoluminescence and includes fluorescence as well as phosphorescence [3]. PL is the optical emission obtained by photon excitation. PL spectroscopy analysis allows non-destructive, contactless characterization of materials. PL has several applications: Band gap and impurity level determination, defect detection, understanding recombination mechanisms and material quality [4, 5].

The measurement of PL is not a simple matter, due to its complexity and very low intensity. Thus specialized techniques and apparatus are required for this metrology. PL can be caused by UV, visible or infrared radiation. A special form of the PL is the anti-Stokes luminescence, where an emission at wavelengths shorter than the shortest wavelength of the excited radiation occurs [3].

A wide variety of ternary layered semiconductors receive much attention due to their optical and electrical features as possible light emitters in optoelectronic device applications from UV to the infrared [3, 6, 7]. The ternary compounds have three different chemical components causing significant physical properties that attracted valuable attention [8, 9].

In recent years, the physical properties of the III-III-VI_2 family, the layer-structured thallium dichalcogenides with chemical formula $TlBX_2$, where B = In or Ga and X = S or Se, have been studied extensively [6]. At room temperature, thallium dichalcogenides belong to the monoclinic system, and their space

group is *C2/c.* The lattice of these crystals consists of alternatively two-dimensional layers arranged parallel to the (001) plane [10]. Each successive layer is rotated by a 90° angle with respect to the previous layer. The fundamental structural unit of a layer is the B_4X_{10} polyhedron representing a combination of four elementary BX_4 tetrahedra linked together by bridging X atoms. The thallium atoms are in trigonal prismatic voids resulting from the combination of the B_4X_{10} polyhedra into a layer. The thallium atoms form nearly planer chains along the [110] and $[1\bar{1}0]$ directions [11]. These crystals are characterized by clearly defined anisotropy in their mechanical properties.

$TlGaS_2$, which is a member of this family of crystals, is a semiconductor with indirect band gap of about 2.46 and 2.55 eV at 300 and 10 K, respectively [12]. In view of its possible applications in optoelectronic devices, a great deal of attention has been devoted to the study of the optical and electrical properties of $TlGaS_2$ [12-17]. In this regard, detailed information on the impurity levels is very useful for the fabrication of high-quality devices. Abutalybov et al. [20] have reported the existence of a fine structure in the PL spectra of a $TlGaS_2$ in the temperature range 1.8-77 K. It was found that the PL lines in the long-wavelength part of the spectrum (595-610) nm were separated by ≈ 0.5 eV from the direct edge exciton absorption peak and were due to recombination of bound excitons. Abdullaeva et al. [21] have observed two broad emission bands in PL spectra of $TlGaS_2$ at T= 6 K due to impurity level-to-band radiative transitions at 499 and 590 nm. Song et al. [16] have investigated the impurity levels of $TlGaS_2$ crystals in the temperature range 90-350 K by thermally stimulated current (TSC) and photoinduced current transient spectroscopy techniques. The activation energies of the observed four peaks were found to be 0.18, 0.23, 0.36 and 0.66 eV. Recently, Yuksek et al. [18] have studied the shallow levels of $TlGaS_2$

crystal in the low-temperature range of 10-60 K by TSC method and observed three trap levels with activation energies 0.006, 0.012 and 0.026 eV. Long-wave optical phonons in $TlGaS_2$ crystals were investigated by infrared reflection and Raman scattering experiments [17, 19].

In this work, we present the results of the PL investigation of $TlGaS_2$ single crystals in the 500-1400 nm wavelength and in the 15-115 K temperature range. The shift of the emission band peak energy as well as the change of the half-width of the emission band with temperature and excitation laser intensity was also studied. The observed results were analyzed using the configurational coordinate (CC) model.

As a part of this thesis, we have also studied the structural characterization of $TlGaS_2$ and $TlInS_2$ crystals. Firstly, we carried out x-ray powder diffraction (XRD) measurements to identify the crystal system and the lattice parameters of these samples.

There are only a few reports in the literature about diffraction data of $TlGaS_2$ and $TlInS_2$. The 2θ and intensities of the peaks of the different reports agree each other but they do not agree on the indexing of the data. Some authors report the system of the crystal to be hexagonal and some others to be monoclinic. We wanted to determine the crystal system of our samples by indexing the data using several relevant computer programs. The crystal system and the lattice parameters of $TlGaS_2$ and $TlInS_2$ were obtained.

Some authors reported phase transitions in the layered crystals at low temperatures. We wanted to learn if such transitions could be observed in our samples using temperature-dependent powder diffraction method. For this reason we obtained the powder diffraction patterns of $TlInS_2$ at low temperatures between 83-250 K. Our observation about this topic will also be presented.

Important information about phase transitions could also be obtained using Differential Scanning Calorimetry (DSC) method. We have obtained DSC patterns of $TlGaS_2$ and $TlInS_2$ at low temperatures. From such patterns we have determined the specific heat capacities and their temperature variations for $TlGaS_2$ and $TlInS_2$, and compared these results with the relevant data in the literature [23-25].

CHAPTER 2

THEORETICAL CONSIDERATIONS

2.1. Introduction

Semiconductors are important class of materials, both for scientific and for industrial applications. Over the last three decades, semiconductors have been used in a wide range of electronic devices, such as transistors, voltage regulators, photocells, photodetectors, and switching devices [26]. Because of the interplay between devices, systems, and networks in integrated circuits, it is important to understand the basic operation and the fundamentals of semiconductors [27]. Besides, the rapid growth of the semiconductor industry has stimulated the demands for better material interpreting and material quality.

In this chapter, we will concern with basic theoretical approaches to be familiar about opto-electronical properties of compound semiconductors in the first two sections. In the third section, we will mention the indexing of x-ray diffraction patterns, and briefly describe the programs that we used. Finally, we present briefly the Differential Scanning Calorimetry (DSC) technique in the last section.

2.2. Electronic properties of semiconductors

Semiconductors exhibit a number of useful and unique properties related to their electronic structure.

2.2.1 Band Structure

A useful way to visualize the difference between conductors, insulators and semiconductors is to plot the available energies for electrons in the materials. Instead of having discrete energies as in the case of free atoms, in solids the available energy states form bands. In solids, the electrons tend to occupy various energy bands. The energy band associated with electrons in their ground state is called the valence band. These electrons are static. The energy band of excited electrons in which they move freely and have usualy higher energy is called the conduction band. Conduction process depends on whether or not there are electrons in the conduction band. As the name implies, electrons in the conduction band are able to conduct electricity. The energy spacing between the valence and conduction bands is called the band gap and corresponds to the energy necessary to excite an electron from the valence band into the conduction band. An electron can not exist there.

Similar to that of insulators, semiconductors have an electronic structure, but with a relatively small band gap, generally less than 2 eV. Since the band gap is relatively small, electrons can be thermally excited into the conduction band, making semiconductors somewhat conductive at room temperature.

2.2.2 Impurity States

Since the presence of impurity atoms largely determine the practical applications of semiconductors, impurities play very important role in semiconductors [28]. When an impurity atom is introduced in a lattice, it causes several types of interactions. The properties of intrinsic crystals can be changed by this kind of atoms. These

impurity atoms may be found in one of two places. Whether they can replace some of the original atoms in the lattice or can occur interstitially among the original ones where its outer-shell electrons are available for conduction. In most cases these impurities enter the lattice by substituting for normal atoms. In this stuation, if the impurity atom replacing one of the constituent atoms of the crystal provides with one or more additional electrons than the atom it replaced, this impurity is called a donor. Si on a Ga-site in GaAs is an example for this. On the other hand, when the impurity atom provides less electrons than the atom it replaces, it forms an acceptor as the role of Si on an As-site in GaAs. This lack of electron due to Si is considered as a hole. Both this hole and the extra electron coming from donor atom are weakly bounded and behave as localized states in each side of the band gap.

When the impurity atom can contribute more than one extra carrier (electron or hole), it is called a multiple donor or a multiple acceptor, both of which have a state for each carrier they can contribute. Apparently, when the multiple donor has released one electron it is singly ionized. When it is doubly ionized, the donor is doubly charged, hence the corresponding binding energy is much greater than for the singly ionized state. Therefore, as the degree of ionization increases, the various donor levels go deeper below the conduction-band edges [29].

2.2.3 Holes in Semiconductors

The most important startling feature that makes a semiconductor so different from a metal is the vacancy *h*, left in the covalent bond by the liberated electron *e*, behaves as if it were a new free particle with a positive electronic charge $+q$ and a mass comparable to that of an electron [30]. This particle is logically called as a hole. This positively

charged vacancy can move, in spite of the fact that the ionized atom itself does not move. Hence, the motion of the hole may be esteemed as a transfer of ionization from one atom to another.

As we know from general electron theory, if we apply an external electric field to the crystal, the electron will have a direction opposite to the field due to the negative charge of the electron simply. On the other hand, if we consider the hole concept, wherever the hole is , a valence electron will fill it by moving in a direction opposite to the electric field with the effect hole drifts in the direction of the field [31].

2.2.4 Extrinsic and Intrinsic Semiconductors

Generally, we can conclude that an intrinsic semiconductor is an insulator at low temperatures and turns to a conductor at high ones, its conductivty tending to increase with temperature. This takes place since in the intrinsic semiconductor the increase in the number of free carriers with temperature far outbalances the reduction of mobility [30]. In a pure semiconductor, a hole is also produced for every conduction electron, and $n = p$ where n and p denotes the concentrations of conduction electrons and holes, respectively. This is called intrinsic conduction and we add a subscript i to n. It is

$$n_i = C^{1/2}\, T^{3/2}\, exp\, (-E_g / 2k_B T). \qquad (2.1)$$

In this formula, the value of constant C depends on the semiconductor material. k_B is Boltzman's constant and T the absolute temperature (at room temperature k_BT = 25.9 meV).

As a matter of fact, the development of practical semiconductor devices would not be possible without the freedom of adding infinitesimal controlled amounts of suitable foreign substances (impurities) to otherwise pure material. By this way, it is possible to create semiconductors exhibiting extrinsic conductivity over a fairly wide temperature range [30]. In this range, these semiconductors may have either more conduction electrons than holes or more holes than electrons. That is, if a semiconductor is extrinsic then $n_o >> p_o$ or $p_o >> n_o$.

2.2.5 Defects

Over several decades, the study of crystalline defects has deduced a considerable impulsion in order to understand the control that is exerted by defects on most technologically significant ptoperties of solids [32]. In general, defects are classified into line defects and point defects. As the name express line defects involve rows of atoms, and typical examples of line defects are dislocations. On the other hand, point defects usually involve isolated atoms in localized regions of a host crystal. Point defects are often further classified into the many kinds with special terminology and notations. These are named as vacancy, interstitial, substitutional, antisite, and Frenkel defect pair. Vacancies and antisite defects are native or intrinsic defects because they do not involve foreign atoms. Their concentrations can not be determined by mass spectrometry or chemical analysis. Besides, defects which involve foreign atoms (i.e., impurities) are referred to as extrinsic defects [33].

The growing importance of compound semiconductors emphasizes the necessity to identify and investigate the properties and the ways so as to control these defects. The vacancies are less mobile in the compound materials than in the

elemental semiconductors. This is reasonable in the sense since diffusion in the elemental materials involves the nearest neighbor moving into the vacancy. However, in the compound materials, it is the next nearest neighbor that must take the move, the nearest neighbor functioning to block its motion [34].

2.3 Optical Properties of Semiconductors

2.3.1 Luminescence

Luminescence is a rewarding field for scientific and practical application. Even though its basic physical mechanism is simple in a conceptual manner, it provides fascinating variety. In 1888, the German physicist Eilhard Wiedemann introduced the term luminescence, of Latin origin, to include both fluorescence and phosphorescence.

The optical processes involve emission of radiation from the sample. Luminescence is one of these processes. In a typical luminescence process electrons in the sample are excited optically or electrically. After some energy relaxation (loss), the excited electrons return to the ground state, during which it emits light [33]. Luminescence is a process where matter generates nonthermal radiation which is characteristic of the particular luminescent material. However, the radiation so generated is also called luminescence so often. In order to avoid the misunderstandings that can arise when radiation and luminescence are used synonymously, luminescence is used to denote either the luminescence process including excitation, emission, and temporary storage of energy, or sometimes just the final emission part of the luminescence process [35]. Furthermore, since the quality and quantity of luminescence

radiation are strongly dependent on the nature of the emitting material, it is useful to begin to study of luminescence with the study of matter.

In addition to the great variety of luminescence emissions from different materials, there are a lot of kinds of input energies which can excite luminescent materials. To distinguish among the different causes of excitation, it has become customary to use prefixes. We can make a list of these methods as follows:

Photoluminescence: Absorption of light

Radioluminescence: High energy particles

Cathodoluminescence: Cathode rays, electron beams

Electroluminescence: Electric fields

Thermoluminescence: Thermally activated ion recombination

Chemiluminescence: Chemical reaction ion recombination

Bioluminescence: Biological processes, usually enzymatic

Triboluminescence: Friction and static forces

Sonoluminescence: Sound and ultrasound

Roentgenoluminescence: High energy x-rays

This list may be extended with other names for luminescence excited by different means [36].

2.3.2 Photoluminescence

In general, photoluminescence is a common method by absorption of photons of energy higher than that of the bandgap, in the resulting process photons of energy

lower than the exciting photons are radiated. When light of sufficient energy is incident on a semiconductor material, photons are absorbed and electronic excitations are created. Eventually, these excitations relax and the electrons return to the ground state. If radiative relaxation occurs, the emitted light is called photoluminescence (PL). This light can be collected and analyzed to yield a wealth of information about the material. The color (or wavelength) of the light provides information on transition energies, and the intensity is a measure of the relative rate of radiative and nonradiative recombination. Radiative transition includes the emission of light but nonradiative does not. Here, we should conclude this: The quantity of the emitted light is linked to the relative contribution of the radiative process.

Optical transitions between two bands are powerfully affected by whether the band structure of the material is indirect or direct. A transition in indirect involves a change in momentum while in direct it does not since the valence band maximum in both cases is at $k = 0$ where k is the wavevector. For the reason that the photon momentum is negligibly small, for an indirect transition, momentum conservation requires the co-operation of another particle. This particle is phonon. It obtains momentum by interacting with a phonon. In the course of the transition, the particle changes its momentum by an amount $\hbar q$. Then the energy conservation formula becomes:

$$h\nu = E_f - E_i \pm E_p \tag{2.2}$$

where E_f and E_i are the final and initial energies respectively and E_p is the energy of

phonon. The minus and plus signs indicate the phonon absorption and emission, respectively.

In direct band gap transition with the same wavevector, semiconductors whose fundamental absorption edge involves a vertical transition are said to have a direct absorption with the following energy conservation relation,

$$hv = E_f - E_i. \tag{2.3}$$

The indirect gap energy is usually determined by the measurement of temperature dependence of the Hall coefficient in intrinsic region, while the direct gap energy is directly measured only in an optical absorption experiment [26]. PL is one of the most useful, powerful, and sensitive optical methods.

As a luminescence process, a PL one involves three individual steps. First, in excitation step, electron-hole pairs have to be excited by an external source of energy. Then the excited electron-hole pairs relax towards quasi-thermal equilibrium distributions. This process is called thermalization. Ultimately, the thermalized *e-h* pairs recombine radiatively to produce the emission in recombination part.

2.3.3 Recombination Mechanisms

Electrons and holes, in a semiconductor, are constantly generated by thermal excitation of electrons from the valence band to the conduction band. Under thermal equilibrium, this generation process is compensated by a recombination process where electrons and holes annihilate each other [26]. Recombination is part of a process to restore equilibrium to a semiconductor that has been perturbed,

or disturbed out of equilibrium. Three things can cause to the perturbations mainly. It can be in the form of an applied electric field, a change in temperature or exposure to light. Recombination takes place when there is an excess of carriers and they are destroyed, by recombining. Remember carriers are in the form of a free electron and hole it leaves behind, or electrons or holes brought in from dopants. When they are destroyed, a negatively charged electron is attracted to the positively charged hole, and as they get together, their charges are canceled and the electron is part of a bond once again.

In order to obtain the general expression for the net recombination rate, we can make the following assumptions: For a single electron transition from a to b, the transition probability, S_{ab}, depends on only a and b states. So as to take place this transition, state a should be occupied with probability p_a and state b should be vacant with probability q_b. Then the general expression for the average rate of the transition from a to b takes the form $S_{ab}p_aq_b$. If we consider the same procedure for the reverse process from b to a, at this time, state b will be occupied and state a will be vacant. Hence the rate of this reverse process is $S_{ba}p_bq_a$. Finally, the net recombination rate per unit volume for the process a to b can then be written as

$$U_{ab} = (S_{ab}p_aq_b - S_{ba}p_bq_a)/V \tag{2.4}$$

Schmidt et al. mention about many recombination mechanisms in their paper [37]. There are four types of recombination which we cover in this study.

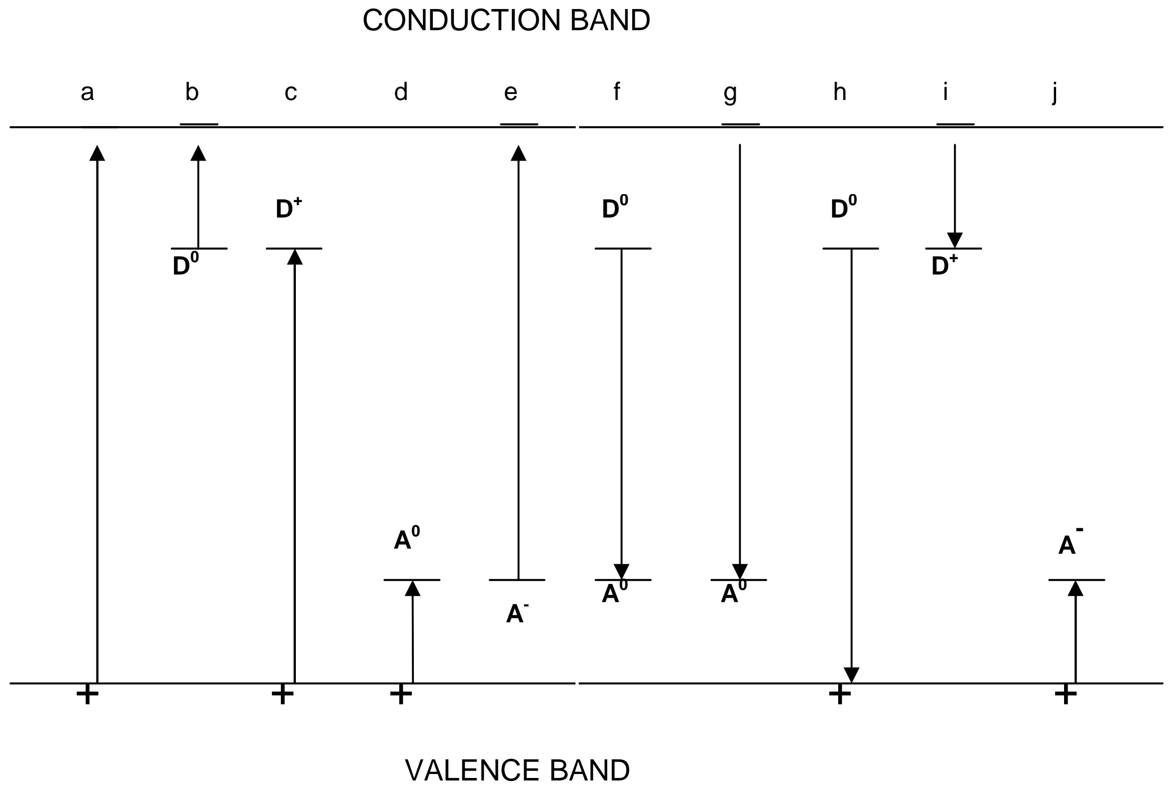

Fig. 2.1: Excitation and Recombination Transitions

2.3.3.a Band-to-band Transition

Band-to-band transition occurs when an electron falls from its state in the conduction band into the empty state in the valence band which is associated with the hole.

This process depends on the density of electrons and holes. The rate is expected to be proportional to the product of n and p, since both carrier types need to be available in the recombination process. The total rate of recombination is given by

$$R = rnp \tag{2.5}$$

as for any bimolecular process, where r is a constant of proportionality. Opposite to the recombination process, there is a constant generation of carriers. However, under thermal equilibrium the recombination rate must equal to the generation rate since there is no net recombination and generation. That is, the generation rate $G = rn_op_o$, where n_o and p_o are thermal equilibrium electron-hole concentration, respectively, must be equal to recombination rate R. The net recombination rate, U, can be expressed as:

$$U = R\text{-}G = r(np\text{-}n_op_o) \tag{2.6}$$

This band-to-band transition is typically also a radiative transition in direct bandgap semiconductors, like GaAs, with a high probability. In an indirect semiconductor, like Si and Ge, recombination can occur radiatively only via phonon-assisted transitions.

2.3.3.b Free-to-bound Transition

Carriers are frozen at sufficiently low temperatures. At higher temperature where all the shallow impurities are ionized, band-to-band transitions tend to dominate. Free-to-bound transitions can occur radiatively or non-radiatively between a free carrier and a charge bound to an impurity. We can consider, as an example, a photoluminescence experiment on a p-type sample containing N_A acceptors per unit volume. Here, at low photoexcitation, the density n_e of free electrons created in the conduction band is much smaller than N_A. These free electrons recombine with

holes trapped on the acceptors. In this example, the emitted photon energy is calculated by E_g-E_A, where E_A is the shallow acceptor binding energy. Therefore, we can use emission due to free-to-bound transitions as a simple way of measuring impurity binding energies.

2.3.3.c Donor-acceptor Pair Transition

Donor-acceptor pair transitions take place in compensated semiconductors. In compensated situation, under equilibrium conditions, some of the electrons from the donors will be captured or compensated by the acceptors. Hence, a compensated material contains both acceptors (A^-) and ionized donors (D^+). It is without questioning assumed that there are more donors than acceptors. By the way, let me point that a semiconductor quite often may contain both donors and acceptors.

By optical excitation, electrons can be created in the conduction band and holes can be created in the valence band. Then these carriers can be trapped at A^- and D^+ sites in order to produce neutral A^o and D^o centers. In returning to equilibrium, a donor-acceptor pair transition (or DAP transition), in which some of the electrons on the neutral donors will recombine radiatively with holes on the neutral acceptors, occur. We can formulate this transition as

$$A^o+D^o = A^-+D^++h\nu. \quad (2.7)$$

We may expect that the photon emitted in a DAP transition has energy

$$hv = E_g - E_A - E_D, \tag{2.8}$$

where E_g is the bandgap energy and E_A and E_D are the acceptor and donor binding energies, respectively. However, the Eqn. (2.8) neglects the Coulomb interaction between the acceptors and ionized donors. This causes a problem. If we suppose the distance between D^+ and A^- to be r, then Coulomb energy will be equal to $-e^2 / (4\pi \epsilon_o^2 r)$, where ϵ_o is the static dielectric constant. By taking account this Coulomb energy, the emitted photon energy should be

$$hv = E_g - E_A - E_D + e^2/(4\pi\epsilon_o^2 r). \tag{2.9}$$

Since the energy of the final state in Eqn. (2.7) is lowered by the Coulomb attraction, the emitted photon energy is increased by the amount $e^2 / (4\pi \epsilon_o^2 r)$ [33].

2.3.3.d Excitons and Bound Exciton Emission

An exciton is a bound state of an electron and a hole in a semiconductor (or an insulator), that is, a Coulomb correlated electron/hole pair. A brilliant picture of exciton formation is as follows: A photon exciting an electron from the valence band to the conduction band enters a semiconductor. The missing electron in the valence band leaves a hole behind, to which it is attracted by the Coulomb force. The exciton is resulted from the binding of the electron with its hole.

Excitons can have a relatively long lifetime because the probability of the electron falling into (annihilating with) the hole is limited by the difficulty of losing the excess energy. We can mention about another limiting factor in the

recombination probability which is the spatial overlap is smaller for lighter electrons, holes and for highly excited hydrogenic states. The existence of exciton states may be inferred from the absorption of light associated with their excitation. In a typical manner, excitons are observed just below the bandgap. Alternatively, an exciton may be thought of as an excited state of an atom or ion.

We expect the photoexcited electrons and holes to be attracted to each other by Coulomb interaction and to form excitons in photoluminescence experiments on high purity and high quality semiconductors at low temperatures. The excitons will be attracted to a small number of donors and acceptors in their neutral state by way of van der Walls interaction when the sample contains these impurities. Neutral impurities are very efficient at trapping excitons to form bound excitons at low temperature since this attraction lowers the exciton energy.

2.3.4 Excitation Power Dependence of Photoluminescence in Semiconductors

The excitation intensity power controls the density of photo-excited electrons and holes, which governs the behavior of these carriers. Each electron and hole recombination has a distinct functional dependence on the carrier density. That the behavior of the photoluminescence intensity alters, as the power of the light source is varied. Hence, it can be used to describe the fundamental recombination process [38]. As a general statement, luminescence intensity I of near band edge photoluminescence emission lines has been found that it is proportional to L^{γ}, as can be expressed:

$$I \alpha L^{\gamma} \tag{2.10}$$

where L is the excitation laser intensity and γ is the dimensionless exponent [39-42]. This γ takes different values: for exciton like transition, it is $1<\gamma<2$ and for both free-to-bound and donor-acceptor pair (D^oA^o) transitions it is less than 1 ($\gamma<1$) [43].

The characteristics of PL observed in experiment can be explained by a model proposed by Schmidt et al. [43]. This model assumes that the hole concentration, p, in the valence band is equal to the electron concentration, n, in the conduction band. Also, thermal separation of free and bound excitons is neglected. Furthermore, this model takes into account all transitions shown in fig. 2.1. In order to identify these transitions the following set of coupled differential equations are used:

$$\frac{dn}{dt} = iL - an^2 - gn(N_D - N_D^0) - enN_A^0 \qquad (2.11)$$

$$\frac{dn_{FE}}{dt} = an^2 + jL - \left[\frac{1}{\tau_{FE}} + \frac{1}{\tau_{FE}^{nr}}\right]n_{FE} - b\, n_{FE} N_D^0 - c\, n_{FE} N_A^0 \qquad (2.12)$$

the term j describes the direct formation of free excitons and can be omitted for laser light energies hv exceeding the gap energy E_g.

$$\frac{dn_{DX}}{dt} = bn_{FE}N_D^0 - \left[\frac{1}{\tau_{DX}} + \frac{1}{\tau_{DX}^{nr}}\right]n_{DX} \qquad (2.13)$$

$$\frac{dn_{AX}}{dt} = cn_{FE}N_A^0 - \left[\frac{1}{\tau_{AX}} + \frac{1}{\tau_{AX}^{nr}}\right] n_{AX} \qquad (2.14)$$

$$\frac{dN_{A^0}}{dt} = h\,(N_A - N_A^{\,0})\,n + i\,(N_A - N_A^{\,0})\,L - c\,n_{FE}\,N_A^{\,0} + \left[\frac{1}{\tau_{AX}} + \frac{1}{\tau_{AX}^{nr}}\right] n_{AX} - d\,N_D^{\,0}\,N_A^{\,0}$$

(2.15)

$$\frac{dN_{D^0}}{dt} = g(N_D - N_D^{\,0})\,n + k\,N_D^{\,0}\,L - b\,n_{FE}\,N_D^{\,0} + \left[\frac{1}{\tau_{DX}} + \frac{1}{\tau_{DX}^{nr}}\right] n_{DX} - d\,N_D^{\,0}\,N_A^{\,0} - f\,N_D^{\,0}\,n,$$

(2.16)

in these equations, N_D and N_D^0 are the concentrations of donors and neutral donors, N_A and N_A^0 are the concentrations of acceptors and neutral acceptors. n_{FE}, n_{DX} and n_{AX} are the concentrations of the free and bound excitons, respectively. τ_{DX}, τ_{DX}^{nr}, τ_{AX} , τ_{AX}^{nr} are the radiative and nonradiative lifetimes of donor and acceptor bound excitons, and τ_{FE} and τ_{FE}^{nr} are the radiative and nonradiative lifetimes of free excitons, respectively. The coefficients a,b,…l are the transition rates of the processes shown in fig.2.1. Since two electron and two hole transitions and the recombination of excitons bound to ionized donors (D^+X) are weak transitions, these are neglected for easiness.

Assuming that, for constant N_D^0 and N_A^0, a small portion of the free electron-hole pairs form excitons and photoexcited carriers recombine by way of defect states of donors and acceptors and neglecting the term an^2 in Eq.(2.11), using Eqn. (2.12) and (2.14), we can derive the luminescence intensities of free and bound excitons, I_{FE}, I_{D^0X} and I_{A^0X}:

$$I_{FE} = \frac{n_{FE}}{\tau_{FE}} = \frac{\beta}{\tau_{FE}}\,n^2 \qquad (2.17)$$

where $n = \dfrac{i}{eN_{A^o} + g\left(N_D - N_{D^o}\right)}$

$$I_{D^0X} = \frac{n_{DX}}{\tau_{DX}} = \frac{bN_{D^0}\beta}{1+\dfrac{\tau_{DX}}{\tau_{DX}^{nr}}}\ n^2 \tag{2.18}$$

$$I_{A^0X} = \frac{n_{DA}}{\tau_{AX}} = \frac{cN_{A^0}\beta}{1+\dfrac{\tau_{AX}}{\tau_{AX}^{nr}}}\ n^2 \tag{2.19}$$

where $\beta = \dfrac{a}{[\ \dfrac{1}{\tau_{FE}} + \dfrac{1}{\tau_{FE}^{nr}}\ ] + b\,N_{D^0} + c\,N_{A^0}}$

and assuming the proportionality between the intensity of free-to-bound transitions and respective transition rates,

$$I_{hD^0} \sim\ n\,N_{D^0} \tag{2.20}$$

$$I_{eA^0} \sim n\,N_{A^0} \tag{2.21}$$

can be written. For fluctuation of N_{D^0} and N_{A^0} with L, assuming that $N_{D^0}N_{A^0}$ is proportional to $I_{D^0A^0}$, they obtained the equation:

$$k_{D^0A^0} = (\ k_{D^0X} - k_{FE}\ ) + (\ k_{A^0X} - k_{FE}\ ) \tag{2.22}$$

for the donor-acceptor pair transition, where $k_{D^0A^0}$, k_{D^0X}, k_{FE} and k_{A^0X} denote the slopes of $\log(I_{D^0A^0})$ vs $\log(L)$, $\log(k_{D^0X})$ vs $\log(L)$, $\log(k_{FE})$ vs $\log(L)$ and $\log(k_{A^0X})$ vs $\log(L)$ graphs.

As a conclusion, we can say that this model can satisfactorily re-create the power dependence of all PL lines. It is not restricted to one particular semiconductor. It can be applied to any direct semiconductor.

2.4 Indexing of Powder X-ray Diffraction (XRD) Patterns

Information about crystal structure is important for most research projects. Relevant information about crystal systems and the lattice parameters can be obtained from the x-ray powder diffraction patterns. X-ray diffraction (XRD) is a non-destructive technique for the qualitative and quantitative analysis of the crystalline materials. Basically, XRD is obtained as the reflection of an x-ray beam from a family of parallel and equally spaced atomic planes. It follows the Bragg's law.

Bragg's law: diffraction takes place if the path of rays reflected by successive planes with distance d is a multiple of the wavelength λ when a monochromatic x-ray beam is incident on lattice planes with an angle θ. The diffraction condition for a beam is given by:

$$n\lambda = 2d\sin\theta \tag{2.23}$$

where n is a positive integer showing the order of reflection maximum, d is the inter-planer spacing between successive atomic planes in the crystal and θ is the angle of reflection. In this formula, Bragg derived a mathematical relation connecting the

wavelength λ of the reflected x-radiation, the spacing d and the angle θ [44].

In structure analysis, XRD is used to investigate the crystallographic structure of a material. The position and the relative intensities of the diffraction lines can be correlated to the position of the atoms in the unit cell, and its dimensions. Structure refinement, simulation, and indexing can be obtained with specific computer programs.

X-ray measurements can be carried out using both single crystal and powder forms of sample. We have used powder form in our measurements. Powder XRD is one of the primary techniques used by solid state scientists to characterize materials; it may provide information about shape and size of the unit cell of the crystal. In powder method, the value of the lattice parameters and the information about the unit cell can be determined accurately. The diffraction peaks in the powder patterns corresponds to the sets of crystal planes that satisfy the Bragg's law. The 2θ values can be related to the wavelength, the lattice parameters and the Miller indices of the plane causing the peaks. Such relations can be expressed for the different crystal systems. By using the row 2θ values of a substance, by carefully analyzing the data one can find the Miller indices of each reflection together with the lattice parameters and the crystal system. This is called indexing.

Theoretically, in order to determine the crystal system of a sample, we should consider the powder diffraction patterns. The system of any crystal must be one of the seven certain crystal systems (cubic, monoclinic, hexagonal, tetragonal, rhombohedral, orthorhombic, or triclinic). At the beginning, we do not know which the relevant crystal system is.

The interplaner spacings can be related to the Miller indices and the lattice parameters. These relations are shown below for the seven crystal system,

For cubic: $$\frac{1}{d^2} = \frac{h^2+k^2+l^2}{a^2} \tag{2.24}$$

For tetragonal: $$\frac{1}{d^2} = \frac{h^2+k^2}{a^2} + \frac{l^2}{c^2} \tag{2.25}$$

For hexagonal: $$\frac{1}{d^2} = \frac{4}{3}\left(\frac{h^2+hk+k^2}{a^2}\right) + \frac{l^2}{c^2} \tag{2.26}$$

For rhombohedral: $$\frac{1}{d^2} = \frac{\left(h^2+k^2+l^2\right)sin^2\alpha + 2\left(hk+kl+hl\right)\left(cos^2\alpha - cos\alpha\right)}{a^2\left(1-3cos^2\alpha+2cos^3\alpha\right)} \tag{2.27}$$

For orthorhombic: $$\frac{1}{d^2} = \frac{h^2}{a^2} + \frac{k^2}{b^2} + \frac{l^2}{c^2} \tag{2.28}$$

For monoclinic: $$\frac{1}{d^2} = \frac{1}{sin^2\beta}\left(\frac{h^2}{a^2} + \frac{k^2sin^2\beta}{b^2} + \frac{l^2}{c^2} - \frac{2hlcos\beta}{ac}\right) \tag{2.29}$$

For triclinic: $$\frac{1}{d^2} = \frac{1}{V^2}\left(S_{11}h^2+S_{22}k^2+S_{33}l^2+2S_{12}hk+2S_{23}kl+2S_{13}hl\right) \tag{2.30}$$

In the above equation V is the volume of unitcell that can be calculated for triclinic systems by:

$$V = abc\sqrt{1-\cos^2\alpha-\cos^2\beta-\cos^2\gamma+2\cos\alpha\cos\beta\cos\gamma} \tag{2.31}$$

where α, β, γ are the angles between lattice parameters *b*, *c*; *a*, *c*; *a*, *b*, respectively,

and $S_{11} = b^2c^2\sin^2\alpha$,

$S_{22} = a^2c^2\sin^2\beta$,

$S_{33} = a^2b^2\sin^2\gamma$,

$$S_{12} = abc^2(\cos\alpha\cos\beta - \cos\gamma), \tag{2.32}$$

$S_{23} = a^2bc(\cos\beta\cos\gamma - \cos\alpha)$,

$S_{13} = ab^2c(\cos\gamma\cos\alpha - \cos\beta)$.

Combining these equations with Bragg law, we can relate 2θ values to the Miller indices for each crystal system. As an example such a relation, for cubic system, is obtained as follows:

$$sin^2\theta = \frac{\lambda^2}{4a^2}\left(h^2 + k^2 + l^2\right) \tag{2.33}$$

If the crystal system is tetragonal with axes *a* and *c*, then the corresponding general equation will be

$$sin^2\theta = \frac{\lambda^2}{4}\left(\frac{h^2 + k^2}{a^2} + \frac{l^2}{c^2}\right) \tag{2.34}$$

and the similar equations can be obtained for the other crystal systems [45].

If all the diffraction lines are considered, then the experimental values of $sin^2\theta$ should form a pattern related to the values of Miller indices (*h*, *k*, and *l*) for the structure. For the cubic system we multiply the $sin^2\theta$ values by a parameter ($4a^2/\lambda^2$) to give

nearly integer values for all the $h^2+ k^2+ l^2$ values. Finally the integer values of $h^2+ k^2+ l^2$ are matched with the *h k l* values to index each plane. This procedure depends on several parameters and rather complex when the crystal system is unknown. In order to determine the Miller indices of diffraction planes, we should consider all the $sin^2\theta$ formulas for each crystal system and choose the most approptiate one. Fortunately, computational techniques can be used to refine powder data. There exist so many powder indexing programs used world wide by crystallographers for indexing powder diffraction data. These programs are typically non-graphical and rely on complex interaction with the user via text file input and output. There is obviously considerable scope for increasing the efficiency of such programs through the use of graphical tools and user interfacing.

In order to analyze the data from the powder XRD measurements, CRYSFIRE indexing packet program was used. It combines several different indexing programs written in FORTRAN by different scientists. The basic features of this packet program will be mentioned next in the Results and Discussion part.

2.5 Differential Scanning Calorimetry (DSC)

Differential Scanning Calorimetry or DSC for short is a technique used to study what happens to crystals when they are heated. It is used to study what we call the thermal reactions taking place in a crystal during heating or cooling. DSC has been used for over forty years to characterize transitions in materials. However, interpretation of the observed events and data by DSC is often very difficult, especially for the inexperienced beginners. Many events, such as crystallization,

melting, annealing, evaporation, etc., which occurs in the sample involves either the absorption or release of heat. The selection of the analysis is difficult and often subjective because many of these processes overlap in temperature.

In the most DSC apparatus, there are two pans, identically positioned platforms and connected to a furnace by a common heat flow path. In one pan, we put the sample, and in the other pan is used as a reference. It is left empty. The device used has a software program to turn on the furnace. It tells to the system to heat the pans with a specific heating rate, as 5, 10, or 15°C per minute. Throughout the experiment, the heating rates through the pans are kept equal and stable.

The pan containing the sample takes more heat compared to the reference pan to increase the temperature at the same rate. Therefore, in a DSC experiment we measure the extra heat induced by the sample. Figure 2.2 illustrates the basic parts of a DSC apparatus.

In a DSC experiment, we obtain a plot of temperature on the x-axis and the difference in heat flow between the sample and reference on the y-axis while the temperature is increasing. At the first glance we can see from this plot the endothermic and exothermic reactions taking place while temperature is changing.

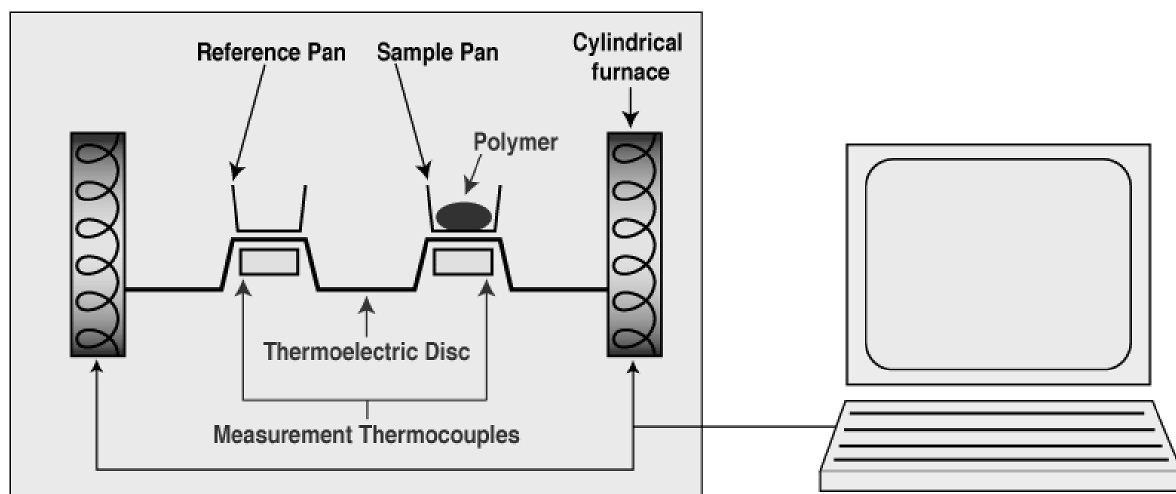

Fig.2.2: DSC setup.

2.5.1 Heat Capacity Determination using DSC

Heat capacity is a measure of the energy that is required to raise the temperature of a material. The heat capacity per amount of substance is the specific heat capacity which is the amount of necessary energy to heat one gram of the material one degree.

C_p is a characteristic thermodynamic property of a material. It should always be positive. Its value at a temperature is independent of the heating rate, and also sample size apart from time-dependent processes. Similar to heating process, how much heat must be removed to cool it to a temperature where the dimensions are stable can be obtained from similar C_p data taken in cooling. C_p value is low for a crystalline material in that molecules can only vibrate. But C_p is higher for liquids in which molecules can also rotate and translate.

DSC provides information to obtain heat capacity. We can achieve capacity measurements between -100 and 725°C with the apparatus that we have used. When

we get the plot of heat flow versus temperature; that is to say, the plot of the heat absorbed or released by crystal versus temperature, we obtain a figure like below.

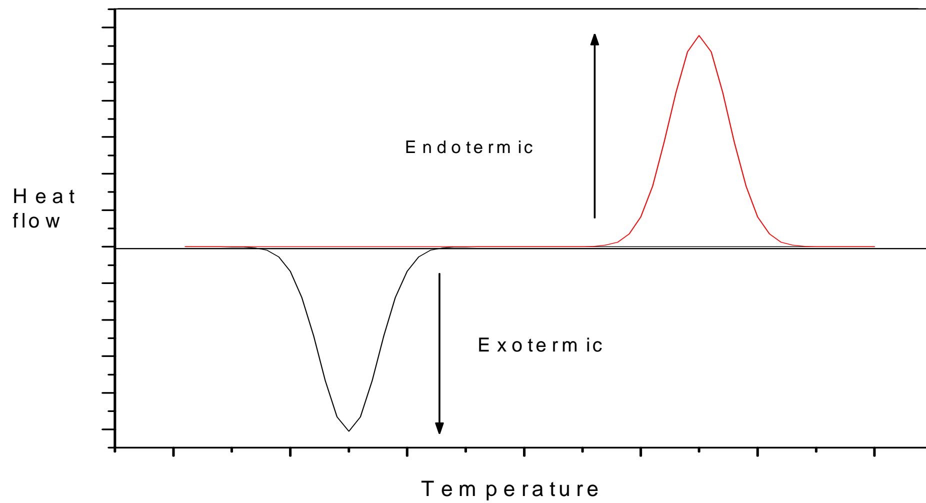

Fig. 2.3: A basic figure of heat flow versus temperature plot.

At a given temperature the heat flow can tell us something. The heat flow is the heat, q supplied per unit time t.

$$\frac{Heat}{time} = \frac{q}{t} = heat\ flow. \tag{2.35}$$

The heating rate is the temperature increase per unit time,

$$\frac{Temperature\ increase}{time} = \frac{\Delta T}{t} = heating\ rate \tag{2.36}$$

If we divide the heat flow q/t by the heating rate $\Delta T/t$ we obtain heat capacity.

$$\frac{\frac{q}{t}}{\frac{\Delta t}{t}} = \frac{q}{\Delta t} = C_p = heat\ capacity\ . \tag{2.37}$$

When a certain amount of heat is supplied into material, its temperature will increase by a certain amount. The amount of heat absorbed to increase temperature by a certain amount is called the heat capacity (C_p). The statements above outline how to obtain heat capacity from the DSC plot.

CHAPTER 3

RESULTS AND DISCUSSION

3.1 Introduction

In this chapter, first, we investigated the details of photoluminescence spectra of $TlGaS_2$ crystals. Second, we analyzed and obtained some results from the data of powder XRD patterns of $TlInS_2$ and $TlGaS_2$ crystals. Also, we attempt to get some conclusions from temperature dependent XRD measurements of $TlInS_2$. Finally, we concluded differential scanning clorimeter (DSC) measurements by finding the specific heat capacities of both $TlGaS_2$ and $TlInS_2$ crystals.

3.2 Photoluminescence Spectra Analysis

In this section, we present the results of the PL investigation of $TlGaS_2$ single crystals in the 500-1400 nm wavelength and in the 15-115 K temperature ranges. The shift of the emission band peak energy as well as the change of the half-width of the emission band with temperature and excitation laser intensity was also studied. The observed results were analyzed using the configurational coordinate (CC) model.

3.2.1 Experimental Details

$TlGaS_2$ polycrystals were synthesized from high-purity elements (at least 99.999%

pure) prepared in stoichiometric proportions. Single crystals of $TlGaS_2$ were grown by the modified Bridgman method. The samples were prepared by cleaving an ingot parallel to the crystal layer, which was perpendicular to the *c*-axis, with typical sample dimensions of 8 x 4 x 2 mm^3. The electrical conductivity of the studied samples was *p*-type as determined by the hot probe method. A "Spectra-Physics" argon ion laser operating at a wavelength 476.5 nm was used as the excitation source. The PL was observed from the laser illuminated face of the samples, in a direction close to the normal of the (001) plane. A "CTI-Cryogenics M-22" closed-cycle helium cryostat was used to cool the crystals from room temperature down to 15 K. The temperature was controlled within an accuracy of 0.5 K. The PL spectra in the 500-860 nm wavelength range were analyzed using a "U-1000 Jobin-Yvon" double grating spectrometer and a cooled GaAs photomultiplier equipped with the necessary photon counting electronics. The PL spectra in the 600-1400 nm wavelength range were obtained by means of “CVI Digikrom DK-480" monochromator and Hamamatsu TE cooled detector. A set of neutral-density filters was used to adjust the excitation laser intensity from 0.35 to 19.49 Wcm^{-2}.

3.2.2 Results and Discussion

Figure 3.2 shows the PL spectrum of the $TlGaS_2$ crystal measured at T = 15 K and excitation laser intensity of 19.49 W cm^{-2} in the 500-1200 nm wavelength range. We

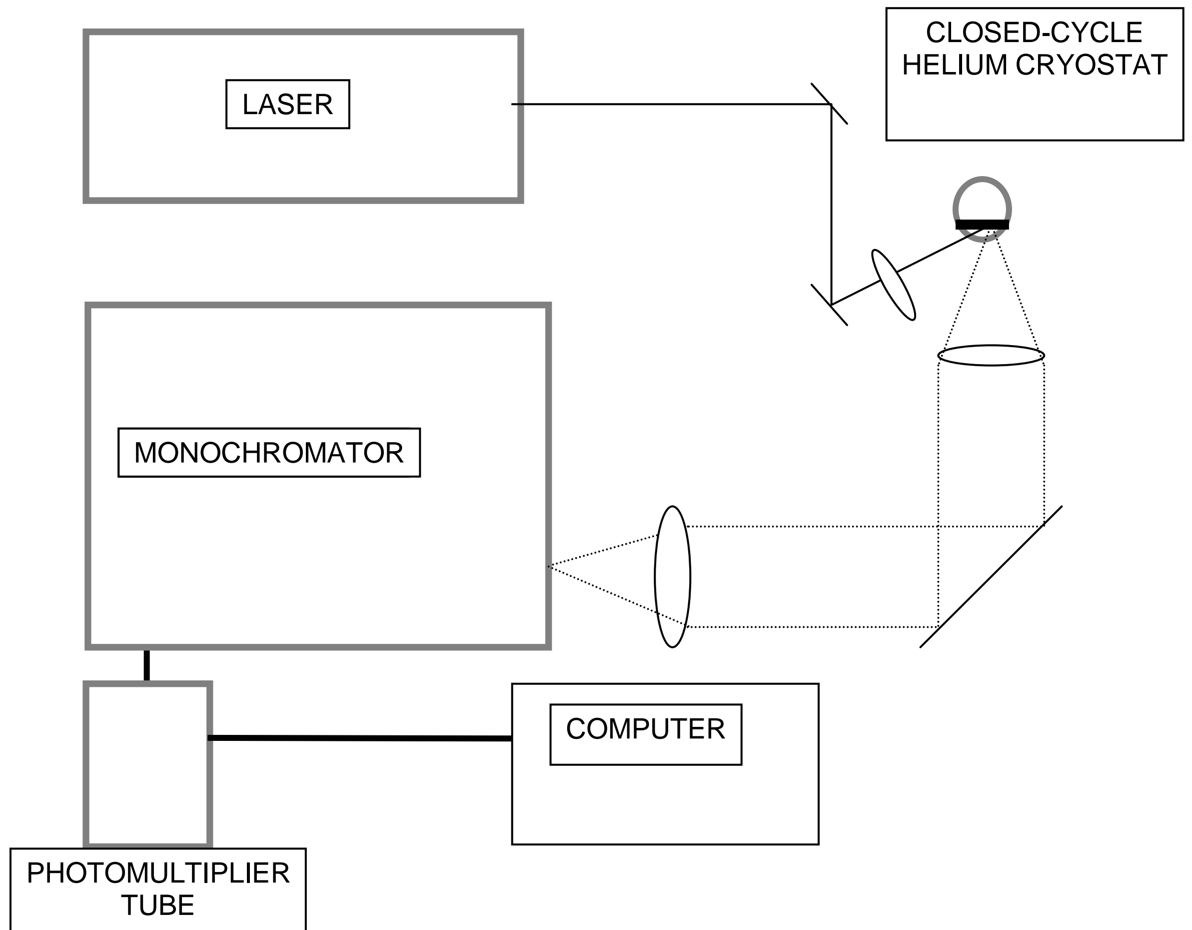

Fig. 3.1 PL setup used in experiments

observed three broad bands with an asymmetric Gaussian lineshapes centered at 568 nm (2.183 eV, A-band), 718 nm (1.727 eV, B-band) and 1102 nm (1.125 eV, C-band) in the PL spectrum. The observed bands have half-widths of 0.221, 0.258 and 0.067 eV for A- , B- and C-bands, respectively. The emission bands intensity, half-width and peak position changed with respect to temperature. These features are typical of emission bands, which are due to donor-acceptor pair transitions observed in ternary semiconductors [46].

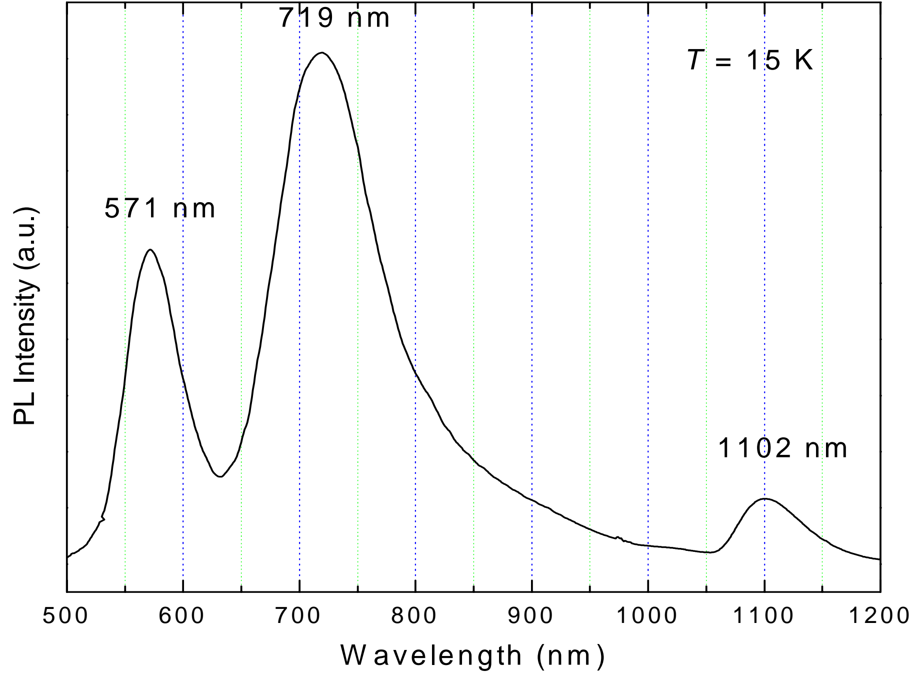

Fig. 3.2: PL spectrum of $TlGaS_2$ crystal in the 500-1200 nm wavelength range at T = 15 K. Excitation laser intensity L = 19.49 W cm^{-2}.

Gasanly et al. [47] presented the results of detailed analysis of the A- and B-bands behavior in the PL spectra of $TlGaS_2$ crystals with respect to the temperature and excitation intensity. It was shown that in the temperature range of 10-90 K, the intensity of the A-band decreases, while the intensity of the B-band increases. For $T > 90$ K, when the A-band becomes very weak, the intensity of the B-band decreases drastically as the temperature increases. The activation energies ΔE_A = 0.005 eV and ΔE_B = 0.085 eV for A- and B-bands, respectively, have been obtained from semilog plots of PL intensities as a function of reciprocal temperature. The A- and B-bands were found to be due to radiative transitions from the deep donor levels located at 0.362 eV (d_1) and 0.738 eV (d_2) below the bottom of the

conduction band to the shallow acceptor levels at 0.005 (a_1) and 0.085 eV (a_2) located above the top of the valence band, respectively. The presence of two acceptor levels allowed to explain the thermal quenching behavior of A- and B-bands in PL spectra of $TlGaS_2$ crystal, where the intensity of the B-band increases in the same temperature range (10-90 K) in which the quenching of the A-band is observed. Quenching of the A-band may be associated with the thermal release of holes from the acceptor level a_1 to the valence band. The thermally released holes are then captured by the acceptor level a_2. Finally, this results in the increase of the intensity of the B-band in the same temperature range where quenching of the A-band occurs.

Figures 3.3 and 3.4 shows the PL spectra of the $TlGaS_2$ crystal (C-band) measured in the 1000-1250 nm near-infrared wavelength range and in the 15-115 K temperature regions at a constant excitation laser intensity of 19.49 W cm^{-2}. From Fig. 3.3 it can be seen that in the temperature range of 15-40 K the intensity of the C-band increases with respect to increasing temperature, while for T > 40 K the intensity of the band decreases. Figure 3.5 shows the temperature dependence of the integrated C-band intensity as a function of the reciprocal temperature in the 15-115 K range. The increase of C-band intensity in the temperature range of 15-40 K may be related to the thermal release of holes from the above-mentioned acceptor level a_1 to the valence band. Probably, these released holes are captured not only by the acceptor level a_2 but also by the acceptor level a_3, which is responsible for appearance of C-band in the PL spectra. The decrease of the C-band intensity in the temperature range of 40-115 K is associated with the thermal release of holes from the acceptor level a_3 when the contribution of captured holes released from level a_1 becomes very small. A rapid thermal quenching of the PL band is observed above T = 60 K. The experimental data for the temperature dependence of the

integrated C-band intensity can be fitted by the following expression [48]

$$I(T) = \frac{I_0}{1 + \alpha_1 T^{3/2} + \alpha_2 T^{3/2} \exp(-\Delta E / kT)} \qquad (3.1)$$

where I_0 is a proportionality constant, ΔE the thermal activation energy, k the Boltzmann constant, α_1 and α_2 are the fitting parameters associated with the temperature dependence of the capture cross sections of the donor and acceptor impurity levels. The best fit in the temperature range 40-115 K using Eqn. (3.1), demonstrated by the solid curve in Fig. 3.5, has been achieved with parameters I_0 = 2.6×10^5, ΔE = 0.035 eV, $\alpha_1 = 1.6 \times 10^{-4}$ and $\alpha_2 = 2.9 \times 10^{-1}$.

In elucidating the nature of luminescence from semiconductors, excitation laser intensity dependence of the PL spectra is an important consideration. In Fig. 3.6, we present the excitation laser intensity dependence of the PL spectra of $TlGaS_2$ crystal.

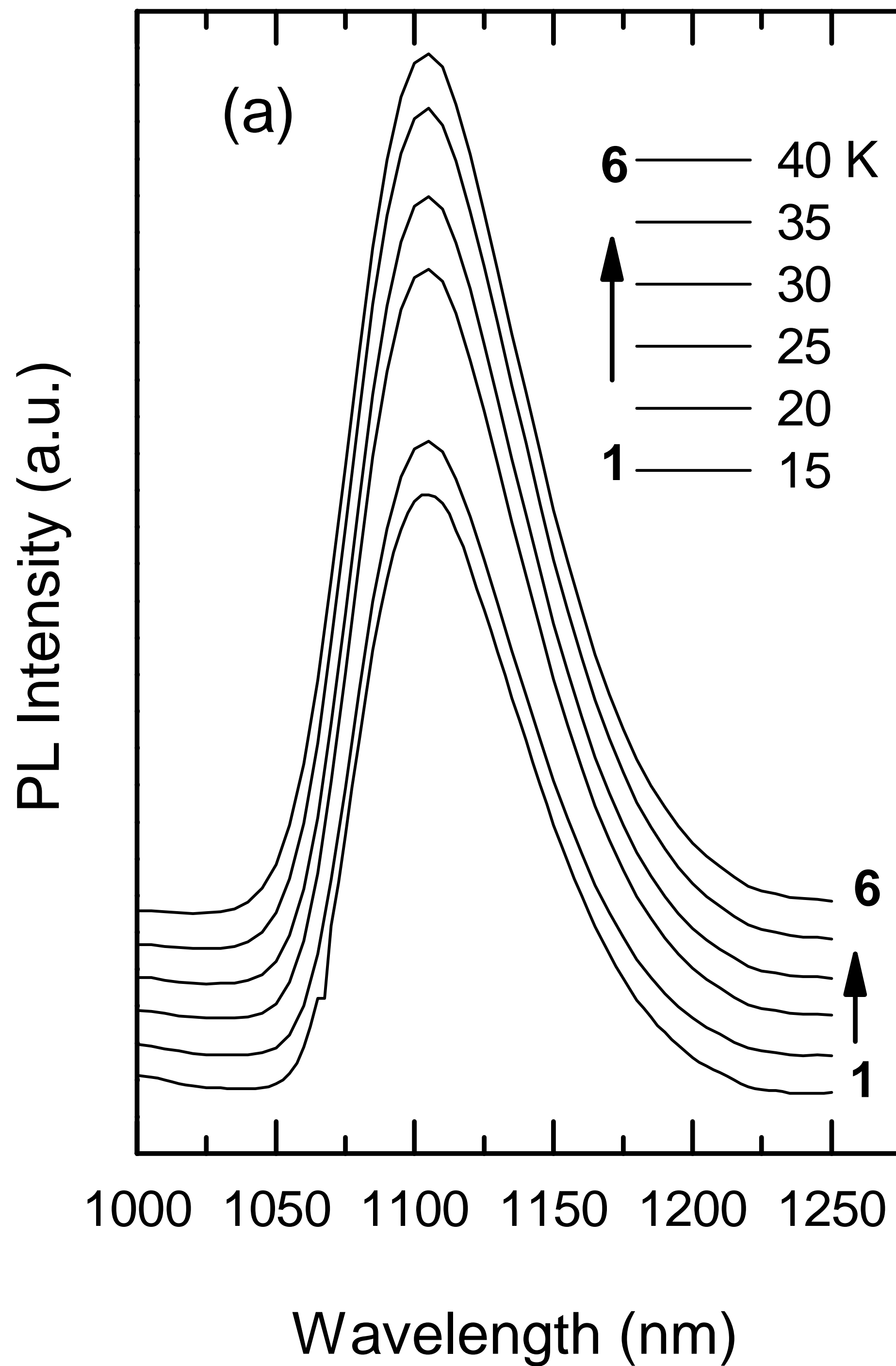

Fig.3.3: PL spectra of TlGaS2 crystal in the 15-40 K temperature range and 1000-1250 nm wavelength region. Excitation laser intensity L = 19.49 W cm^{-2}

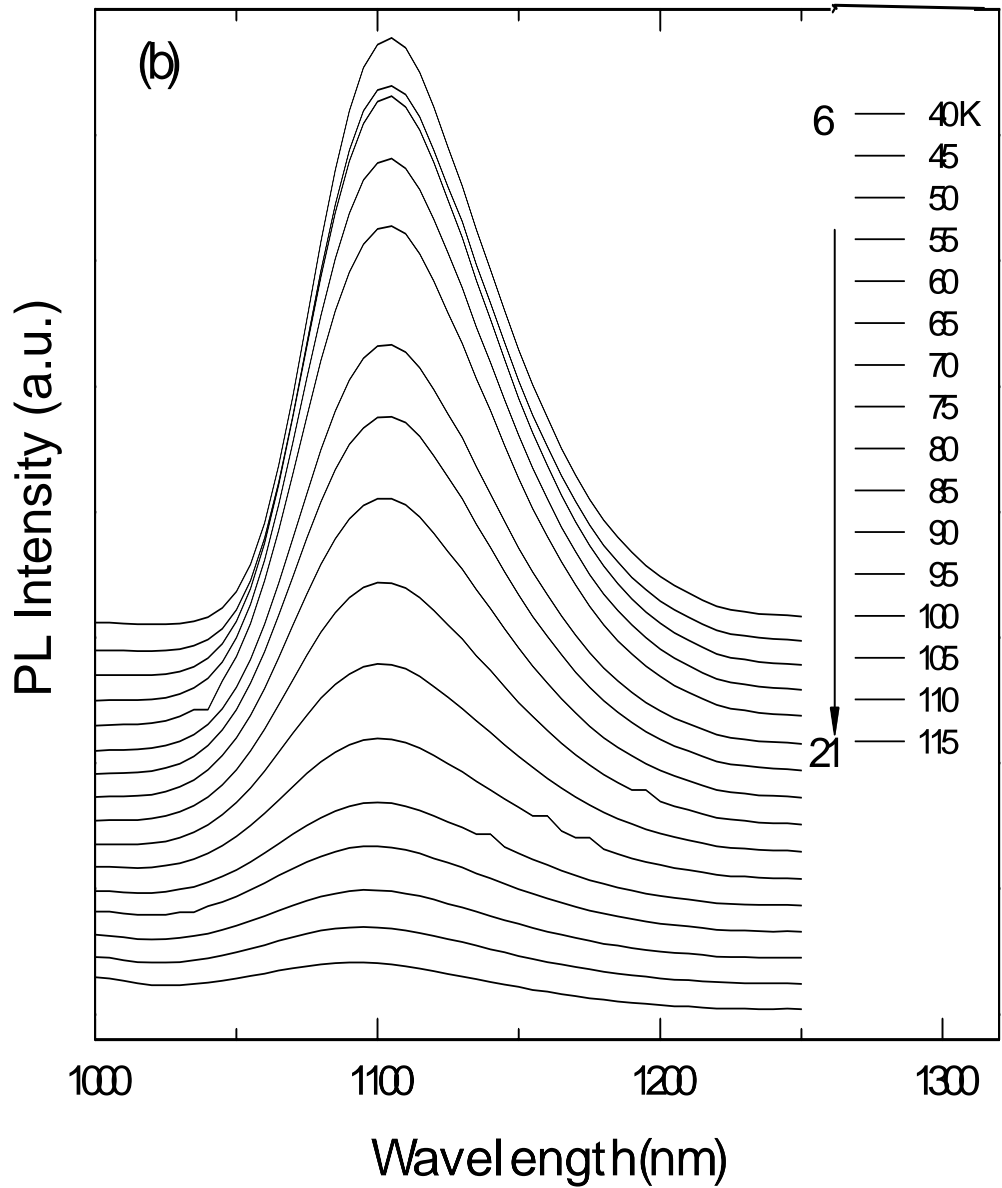

Fig. 3.4: PL spectra of TlGaS2 crystal in the 40-115 K temperature range and 1000-1250 nm wavelength region. Excitation laser intensity L = 19.49 W cm^{-2}.

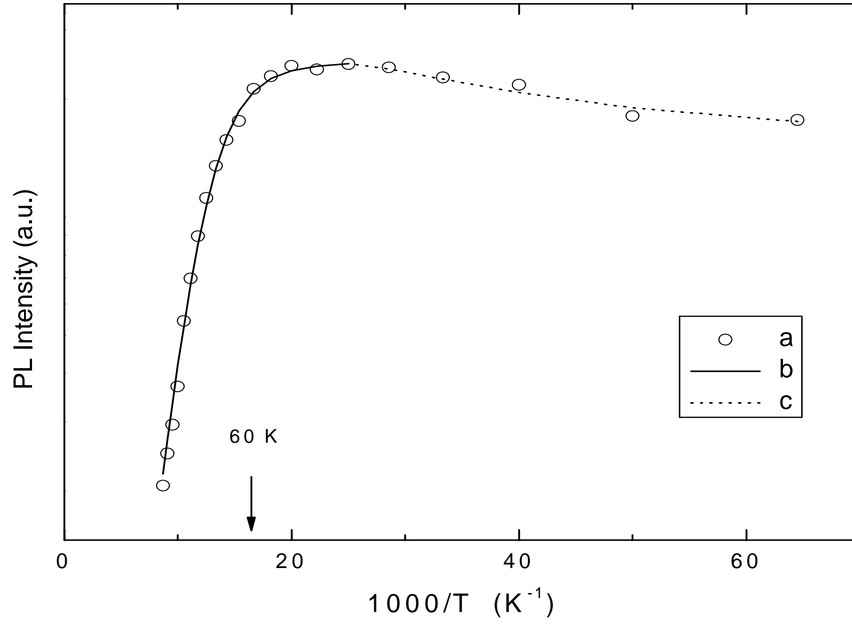

Fig. 3.5: Temperature dependence of integrated PL band intensity for $TlGaS_2$ crystal. The arrow at T = 60 K shows the starting point of the intensive quenching process. (a) are the experimental data, (b) gives the theoretical fit using equation (3.1), (c) is only the guide for eye.

The C-band is visible even at the lowest excitation intensity and increases in intensity as the excitation intensity increases. Detailed analysis of the peak position of this band as a function of increasing excitation laser intensity did not yield any variation of the peak energy values. We, therefore, concentrated on the analysis of PL intensity as a function of the excitation laser intensity. The experimental data can be fitted by a simpler power law of the form:

$$I \propto L^{\gamma}, \qquad (3.2)$$

where I is the PL intensity, L is the excitation laser intensity and γ is a dimensionless exponent. It was found that the integrated intensity of the emission band increases sublinearly with respect to the excitation laser intensity (Fig. 3.7). The value of γ was found to be 0.97. It is well known that for excitation laser photon with an energy exceeding the band gap energy, E_g, the coefficient γ is generally $1 < \gamma < 2$ for the free- and bound-exciton emission, and $\gamma \leq 1$ for free-to-bound and donor-acceptor pair recombination [49]. Thus, the obtained value of $\gamma < 1$ further confirms our assertion that C-band in the PL spectra of $TlGaS_2$ is due to donor-acceptor pair recombination.

Peak energy of C-band does not change with increasing excitation laser intensity (Fig. 3.6). This result rules out the model of "distant" donor-acceptor pair (DAP) recombination process where a shift toward higher energies are expected as the excitation laser intensity is increased [50]. It is known that in general, the emission energy from a DA pair separated by a distance of r is obtained from [51]

$$E(r) = E_g - (E_A + E_D) + \frac{Z_D Z_A e^2}{\varepsilon r} , \tag{3.3}$$

where, E_g is the band gap energy, E_A and E_D are the acceptor and donor ionization energies, ε is the dielectric constant, Z_D and Z_A are the charges of the donor and acceptor states, respectively.

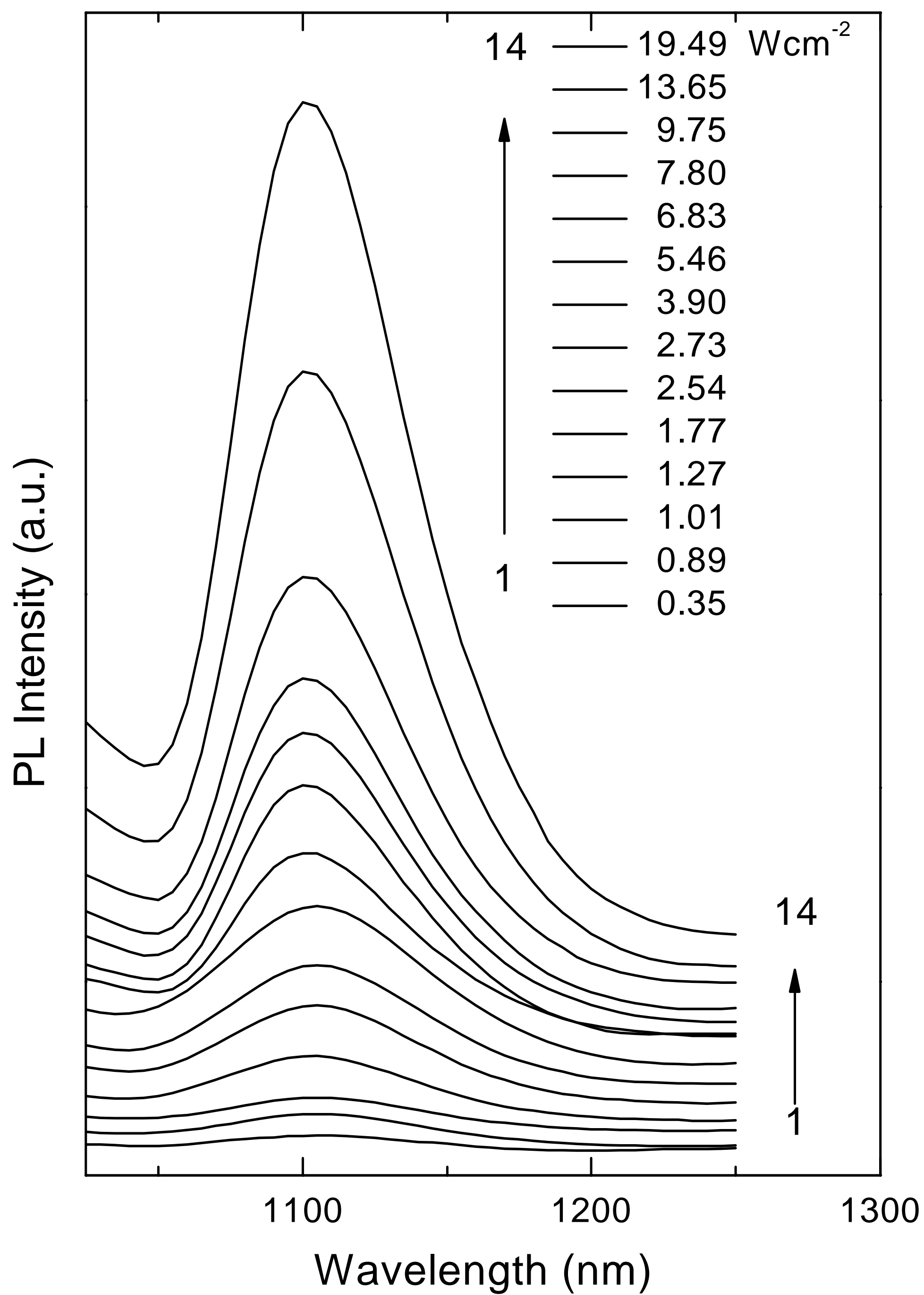

Fig. 3.6: PL spectra of TlGaS2 crystal as a function of excitation laser intensity at T = 15 K.

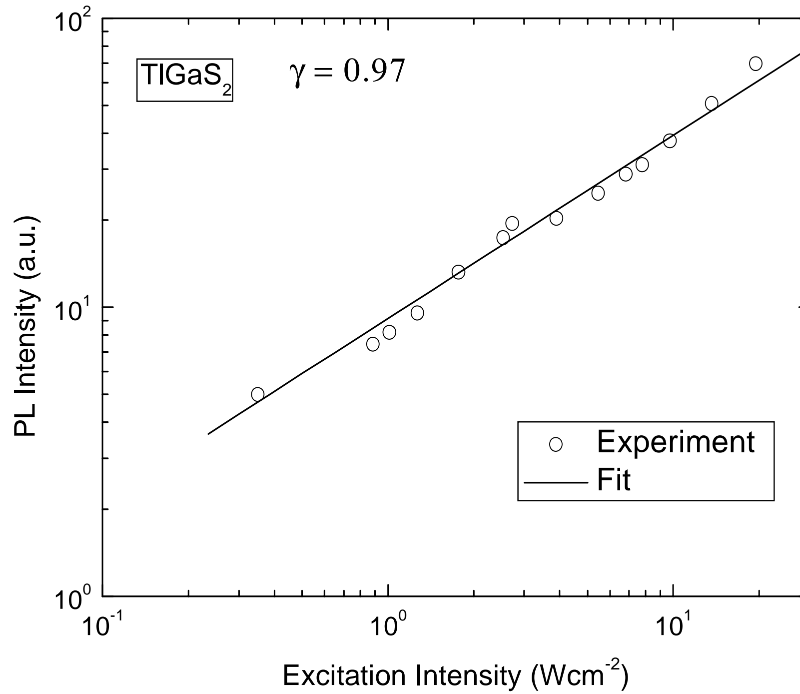

Fig.3.7: Dependence of integrated PL band intensity on excitation laser intensity at T = 15 K. The solid curve gives the theoretical fit using Eqn. (3.2)

From Eq. (3.3), it is clear that as the excitation laser intensity is increased, the contribution of closer pairs will increase leading to the expected blue shift of the peak energy of the emission. Since this is in contrast with the observed data, we conclude that, only close pairs such as the nearest or next-nearest neighbors are involved in the transitions.

Figure 3.8 shows the shift of the emission peak energy as a function of temperature. The emission band peak energy increases with increasing temperature. This is opposite to the behavior of the band gap energy shift, which decreases with increasing temperature [58]. The total range of the peak energy shift is 0.014 eV. Similar behavior for the peak energy shift as well as the above-mentioned half-

width increase with temperature has been observed for the emission bands of *p*-GaAs [52] and layered *p*-GaSe [53]. The 1.37 eV (GaAs) and 1.20 eV (GaSe) emission bands were associated with a vacancy-acceptor complex center, and the recombination mechanism was interpreted as self-activated luminescence in terms of the CC model. Since the CC model was so successful in explaining the behavior of the luminescence associated with such a localized center in layered *p*-GaSe, it was also applied here for layered TlGaS2 which belongs to the same III-VI family as GaSe with a layered crystal structure.

Figure 3.9 presents the temperature dependence of the C-band half-width W, which appears to follow the CC model equation [54]

$$W = W_{\mathrm{o}}\ [\coth(h\nu_{\mathrm{e}}/2kT)]^{1/2}\,, \qquad (3.4)$$

where W_{o} is a constant, whose value is equal to W as the temperature approaches 0 K, and $h\nu_{\mathrm{e}}$ is the energy of the vibrational mode of the excited state. The half-width measurements were not performed above 115 K, because of the reduced PL intensity. However, the changes in the half-width between 15 and 115 K are large enough to show the functional dependence of Eq. (3.4). The solid line in Fig. 3.9 is a plot of Eq. (3.4) with parameters W_o = 0.071 eV and $h\nu_e$ = 0.011 eV.

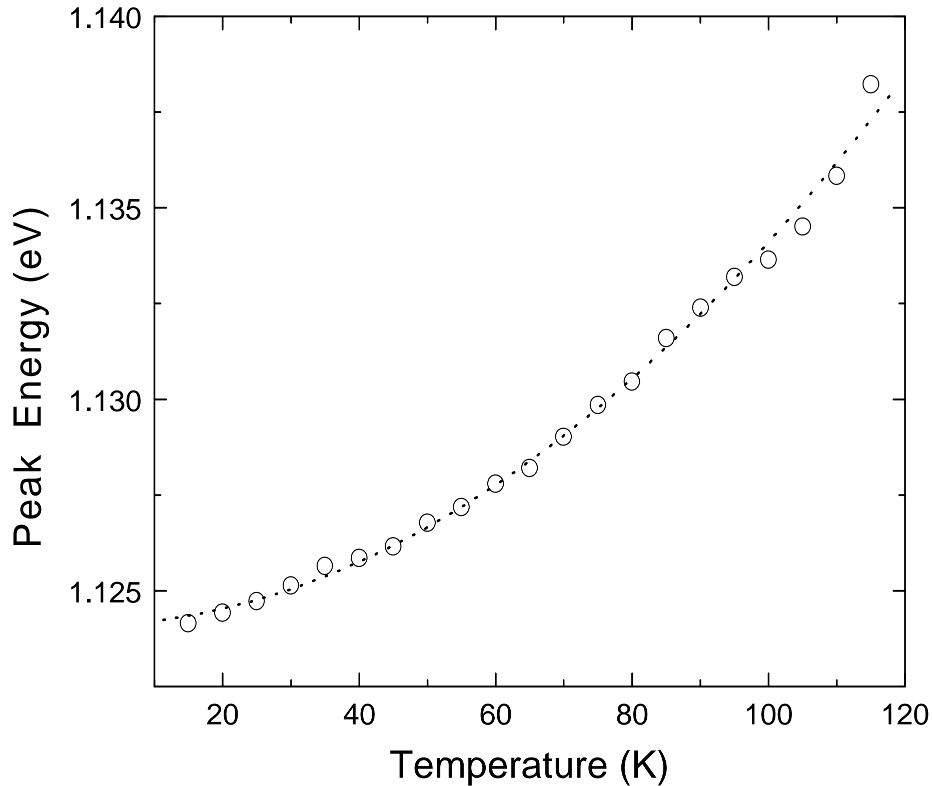

Fig.3.8: Temperature dependence of the emission band peak energy for $TlGaS_2$ crystal. The dotted line is only guide for the eye.

The fact that the excited state vibrational energy ($h\nu_e$) is lower than the LO phonon energy of 0.039 eV (315 cm^{-1}), measured by IR reflection [59], shows the localized nature of the centers and the validity of applying the CC model [52].

Figure 3.10 shows the CC model for the $TlGaS_2$. Following the *p*-GaAs [52] and *p*-GaSe [53] works, let us assume that, the ground state of the localized center is derived from an acceptor level a_3, the excited state originates from a sulphur vacancy donor level d_3, and the zero point of both states lie within the band gap. Actually, in compound semiconductors a deviation from stoichiometry generates donors for the case of anion vacancy [55].

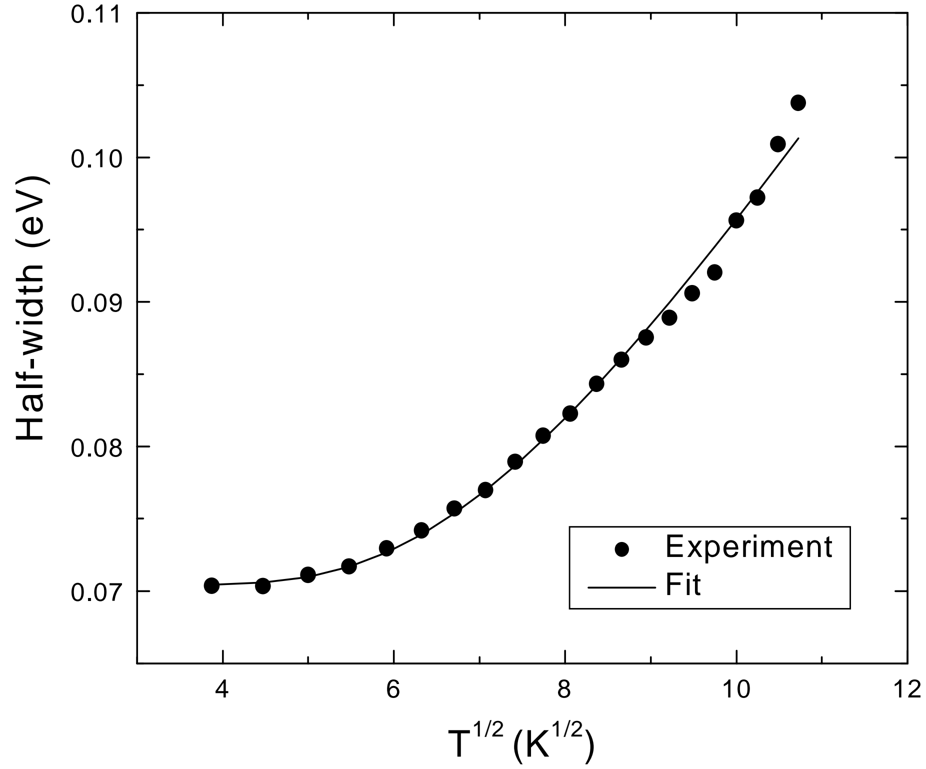

Fig.3.9: Variation of the half-width with square root of temperature for $TlGaS_2$ crystal emission band. The solid curve is a plot of Eqn. (3.4) with $h\nu_e = 0.011$ eV.

The acceptor level a_3 above the top of the valence band may be linked, as in GaSe [56], to the defects and stacking faults, which are due to the weak interlayer interactions in the studied crystals. Electron transitions from the excited state of the donor level to the ground state of the acceptor level gives rise to the PL with emitted photon energy E_{ems}. Also, according to the CC model, when the ground-state vibrational energy is larger than the excited-state vibrational energy, the peak shift of the emission band with temperature is opposite to the band gap energy shift [52].

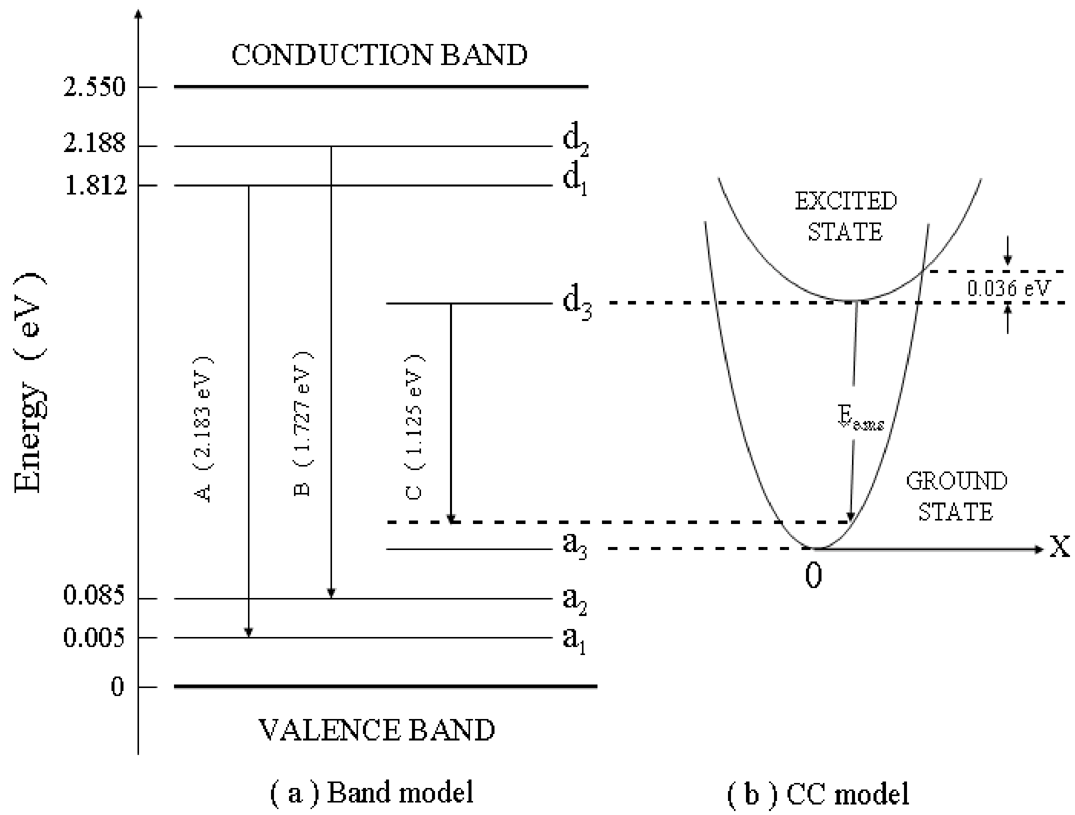

Fig.3.10: Band model (a) and configurational coordinate (CC) model (b) of TlGaS2 crystal at $T = 15$ K.

In terms of the CC model, the observed quenching of the C-band in the PL spectra with increasing temperature (Figs. 3.4 and 3.5) is due to an increased electron population of the excited state at higher displacement coordinates. These electrons then return to the ground state through nonradiative recombination. Thus, the activation energy $\Delta E = 0.035$ eV, obtained from the thermal quenching of the PL , is the difference in the energies of the lowest excited state and the intersection point of the excited and the ground state CC curves (Fig.3.10).

3.3 Results of XRD Measurements

X-ray powder diffraction measurements were carried out to identify the structural features of $TlInS_2$ and $TlGaS_2$ samples. CuKα radiation (λ = 1.540598 A^o) was used in the scan range of 2θ = 5-80°. In order to analyze the diffraction data, we have used CRYSFIRE Powder Indexing System. Analyzing the diffraction data means indexing the diffraction peaks (finding the Miller indices of the diffraction planes) and determining the crystal system and the lattice parameters.

CRYSFIRE: It is a system of programs. Its function is to provide a set of tools to assist in the preparation and enhancement of powder diffraction data for indexing. In particular, it acts as an expert system to allow relatively fast indexing to be carried out by a non-specialist.

When an indexing command is activated, control passes to the accessory scripts, to run a sequence of programs carrying out indexing. The program displays the most proper results, and finally returns to CFmain (CRYSFIRE main prompt) and the CRYSFIRE command prompt.

There are 11 different programs inside CRYSFIRE packet. Each of them has individual role of use. These are Ito, Dicvol, Treor, Taup, Kohl, Fjzn6, Lzon, Losh, Mmap, and ClePage.

- For high symmetry systems as cubic, tetragonal, and hexagonal Taup and Dicvol91 appear to be suitable.
- Other moderately fast programs applicable for any crystal system are the index-space programs Kohl and Treor90

- For low symmetry cells down to monoclinic, the Dicvol91 low symmetry mode 2 is efficient, but it does not allow any impurity lines.
- Most of these indexing programs require at least 20 diffraction peaks.

To obtain acceptable results, the data quality is the most significant point. All the precautions should be taken to produce accurate diffraction data. Before we analyze our data, we applied the programs using the data of some well known structures, taken from JCPDS files, to make sure that the program leads to the expected results.

Fig. 3.11 indicates the powder XRD patterns of $TlInS_2$. There are several different crystal data files for $TlInS_2$ in literature. The structure of $TlInS_2$ crystal is reported to be hexagonal modifications with lattice parameters a = 3.81 A^o and c =14.91 A^o (89-3961, 88-2412) or a = 3.83 A^o and c = 14.88 A^o (65-1975, 74-3000) in four of them. Two of these files state the crystal system to be rhombohedral with lattice parameters a= 7.730 A^o and α = 28.60° (85-0636) or a = 3.83 A^o and c = 22.23 A^o (65-2110).

Even though our peak positions correspond well to those of the results reported in literature, we could not obtain the hexagonal or rhombohedral structures with proposed lattice parameters using the CRYSFIRE packet program. In fact, except TREOR90 no other programs gave the above stated results for our data. TREOR90 leads to tetragonal system with lattice parameters a = 14.88 A^o and c = 4.46 A^o. Hence, we tried to concentrate on TREOR90 to compare our results with the literature values and also to check the accuracy of the indexing program. TREOR90 runs according to some parameters for indexing accuracy that are D1 and D2. The program assigns the default values D1= 0.0002 and D2= 0.0004. By changing these values as D1 = 0.0004 and D2 = 0.0006, we obtained hexagonal system with lattice

parameters a = 3.83 A^o and c = 14.88 A^o, that is, the proposed structure and lattice parameters given in the powder diffraction data file numbers 65-1975 and 74-3000 for $TlInS_2$. This coherence between our result and the results in the files 65-1975 and 74-3000 help us to choose efficient parameters for the TREOR90 program.

For $TlGaS_2$, we could not find any diffraction data file in the softwares. There is only one set of reference data given by Hahn et al. [22]. They state the structure to be monoclinic with lattice parameters a = 10.31, b = 10.43 and c = 15.07 A^o with β = 99.60°.

We have obtained the diffraction pattern of $TlGaS_2$ as shown in Fig. 3.12. For this pattern, the result obtained from the TREOR90 program was monoclinic with lattice parameters a = 9.62, b = 4.01, and c = 7.52 A^o with β = 96.30°. At first glance, these values do not agree with Hahn's results. However, we have noticed that Hahn's a and b parameters are very close to the diagonal of the present *a* and *b* values. Also twice of our *c* value is nearly equal to Hahn's c value. The relative intensities, 2θ and d values, corresponding Miller indices, and the lattice parameters of observed reflections of $TlGaS_2$ are given in Table 3.1. Based on the available programs and their outputs with our data (2θ values) we propose the indexing presented in Table 3.1 to represent the best and relevant indexing for $TlGaS_2$.

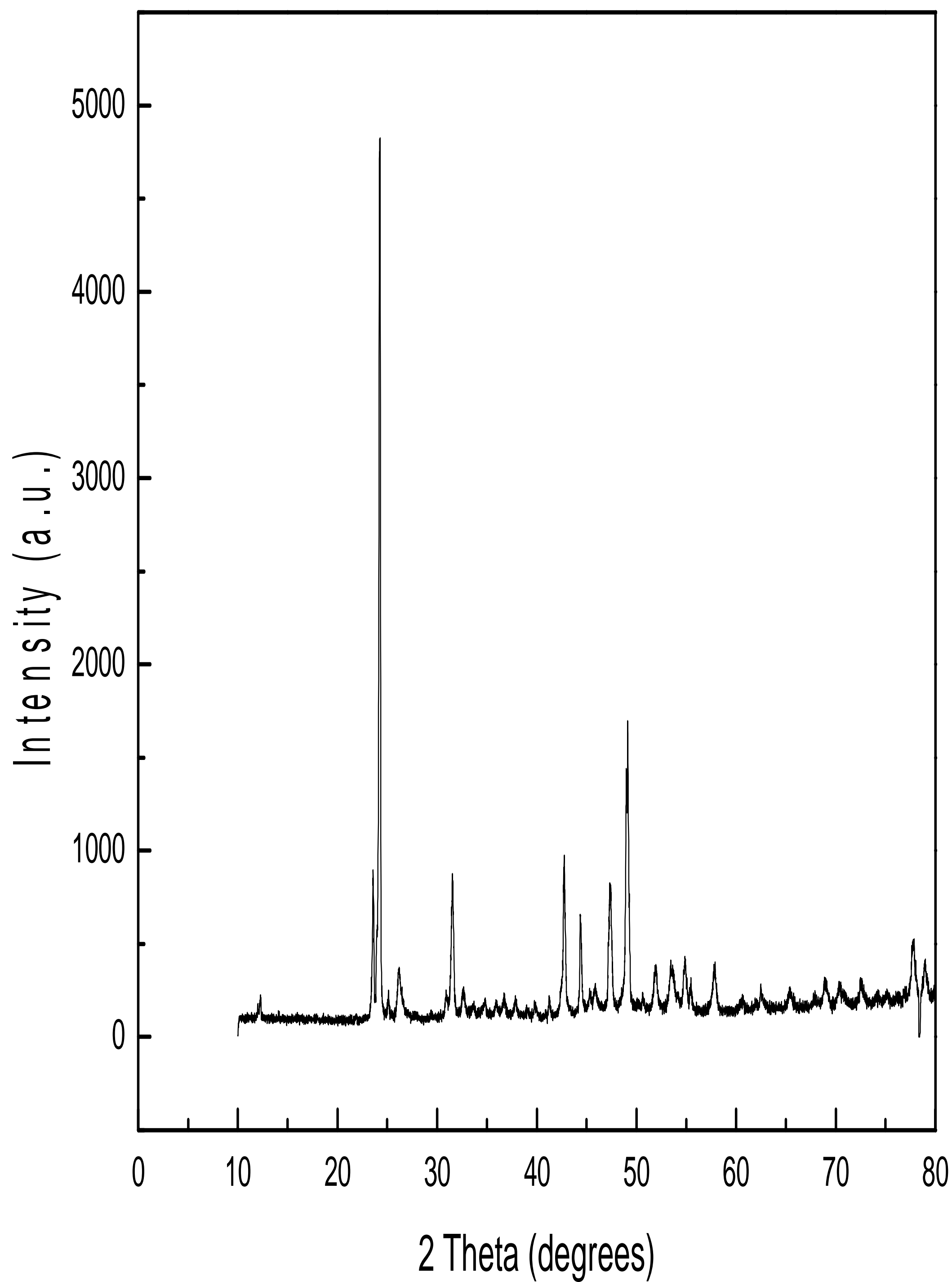

Fig.3.11: X-ray powder diffraction pattern of $TlInS_2$.

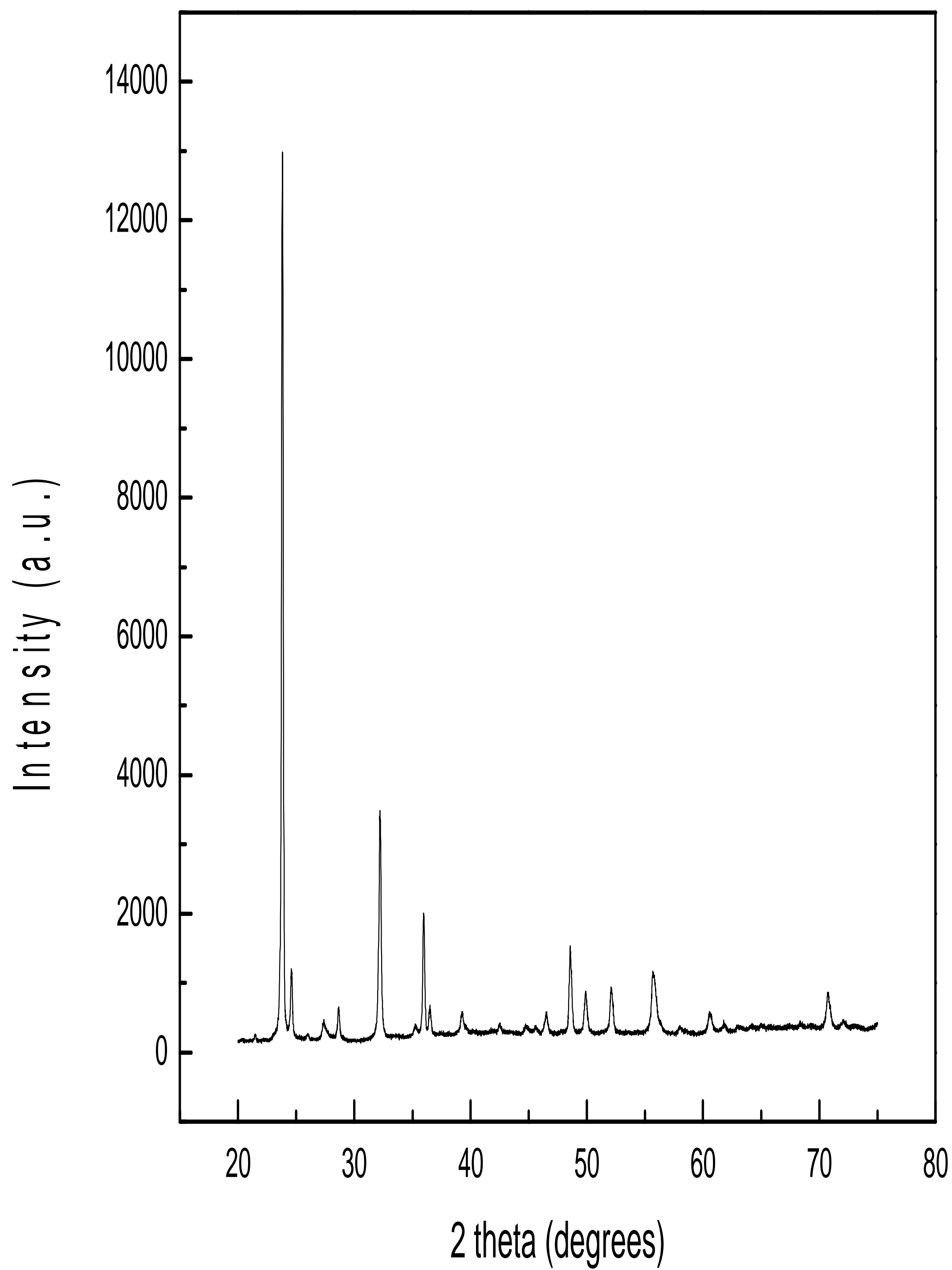

Fig.3.12: X-ray powder diffraction pattern of $TlGaS_2$.

Table 3.1: The TREOR90 outputs from the x-ray diffraction measurements of $TlGaS_2$.

System: Monoclinic Unit cell volume = 288.49 A^3 a = 9.62 A^o b = 4.01 A^o c = 7.52 A^o β = 96.30^o.				
h k l	No.	2Theta (in deg.)	d-Value	Intensity I/I_o
0 0 2	1	23.800	3.7354	100
-1 0 2	2	24.580	3.6186	10
1 1 1	3	27.340	3.2592	3
-2 0 2	4	28.630	3.1153	5
2 1 1	5	32.190	2.7784	28
3 1 0	6	35.950	2.4959	17
-2 1 2	7	36.480	2.4609	5
2 1 2	8	39.240	2.2939	5
-1 0 4	9	48.560	1.8732	13
-4 0 3	10	49.870	1.8270	7
-1 2 2	11	52.090	1.7543	8
-2 1 4	12	55.670	1.6496	10
-6 0 2	13	60.550	1.5278	4
-7 0 2	14	70.720	1.3310	8

3.4 Temperature Dependent XRD Measurements

Temperature dependent x-ray diffraction is one of the most powerful analytical methods to study the phase transitions during temperature treatments of a sample. The combination of a reliable, fast, temperature monitoring and control with the capability of recording a wide 2θ range opens new analytical possibilities for laboratory XRD experiments.

Sheleg et al. [57] reported some extra low intensity diffraction peaks of $TlInS_2$ in the 2θ range of 40-45°. The extra peaks symmetrically located on the right and left of the main peak near $2\theta = 44.4^o$. They interpreted these extra peaks to be associated to a so-called commensurate and incommensurate phase transitions. The lattice demonstrates additional symmetry with repeat distances related to the original lattice parameters. This additional symmetry is labeled as “super periodicity”. We were interested to see if our sample would show evidences for such a phase transitions. For this reason we have carried out powder diffraction measurements at low temperatures.

Figures 3.13, 3.14 and 3.15 show the diffraction patterns of $TlInS_2$ at different temperatures from 80 to 250 K. Examination of these patterns indicates that our sample do not go through a phase transition at low temperatures as reported in [57]. The differences of the growth conditions and amounts of impurities may be effective for the occurrence of the transitions at low temperatures.

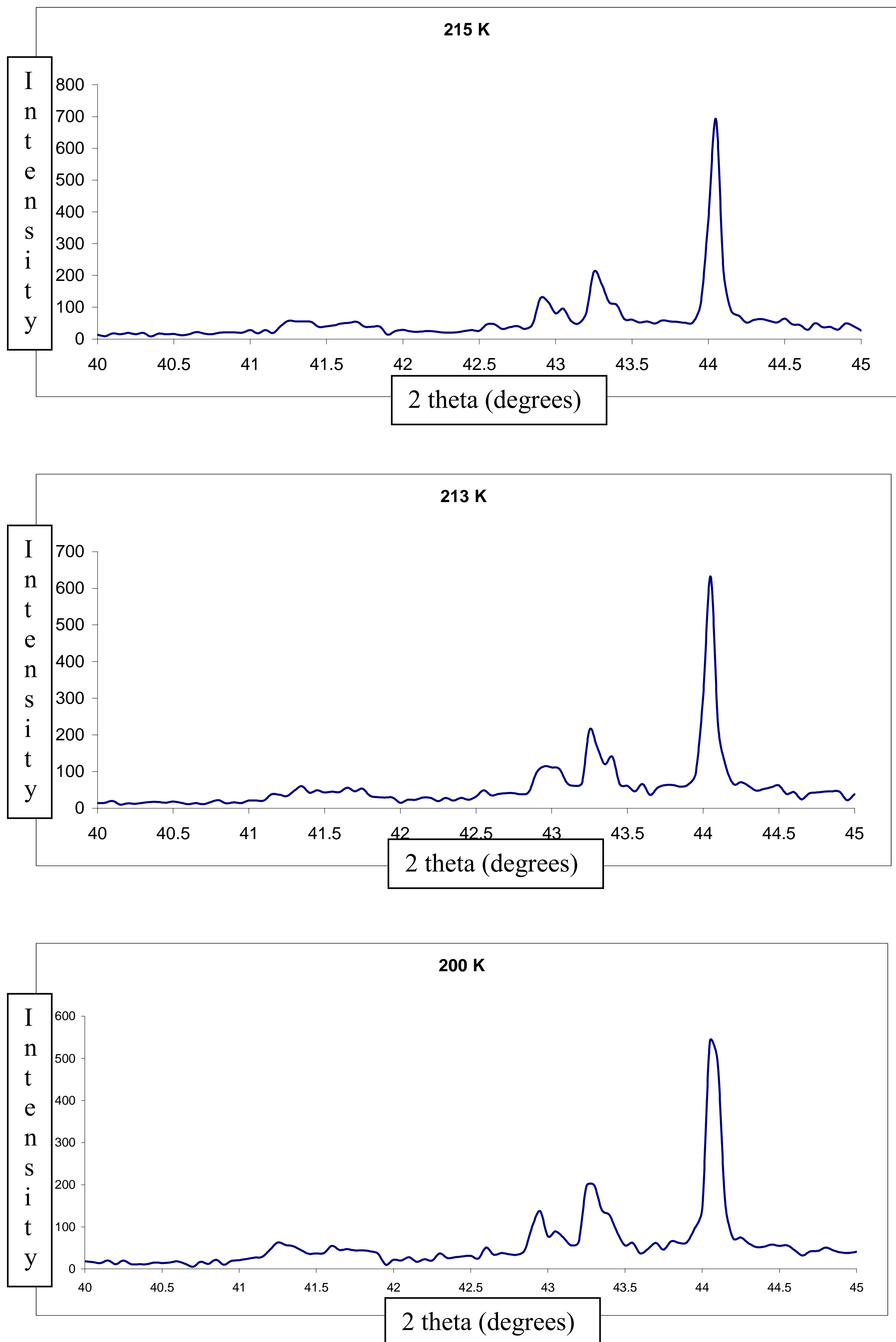

Fig. 3.13: Fragments of diffraction patterns of the $TlInS_2$ crystal at various sample temperatures T, 215, 213, and 200 K, from top to down.

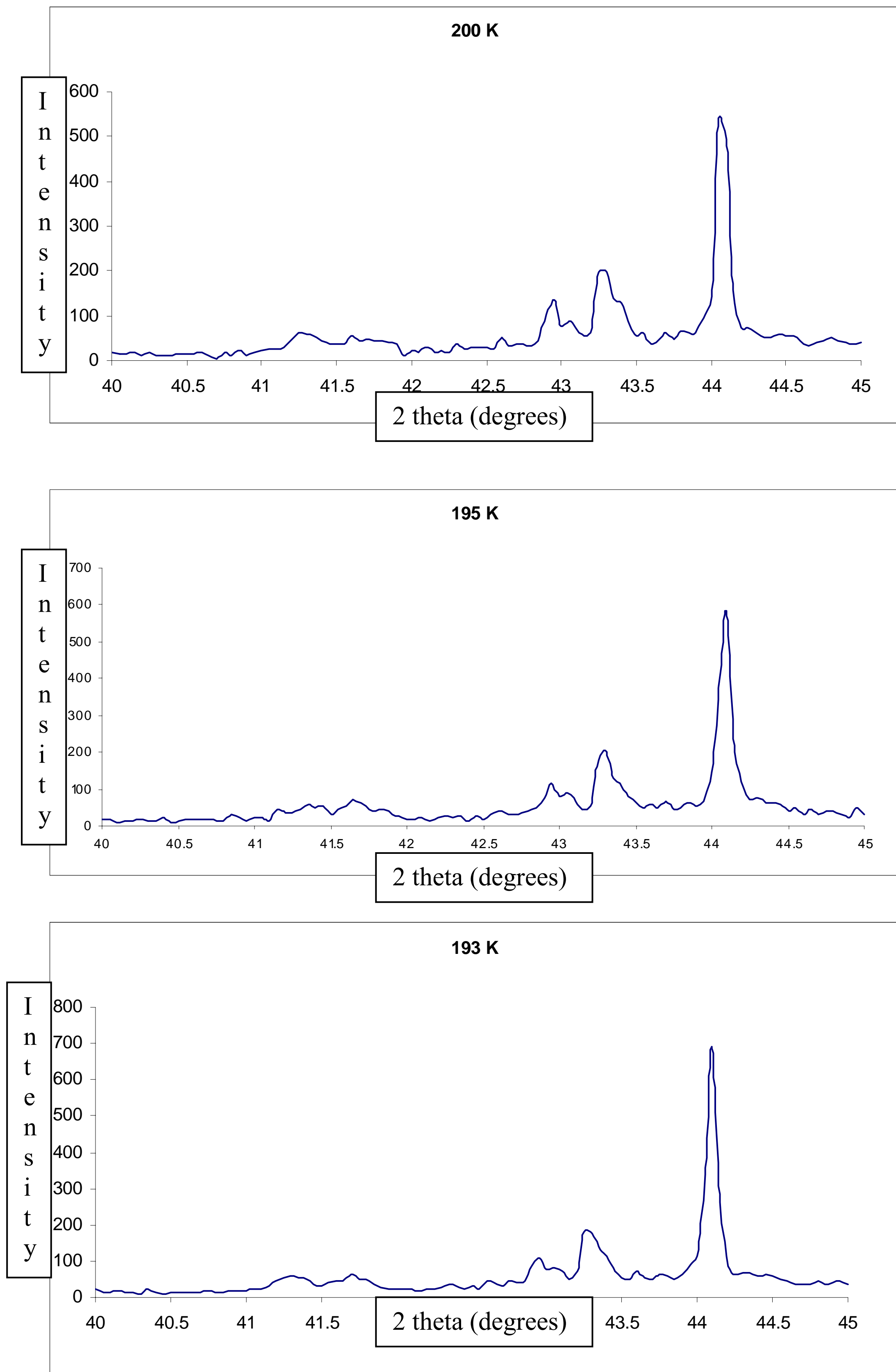

Fig.3.14: Fragments of diffraction patterns of the $TlInS_2$ crystal at various sample temperatures T, 200, 195, and 193 K, from top to down.

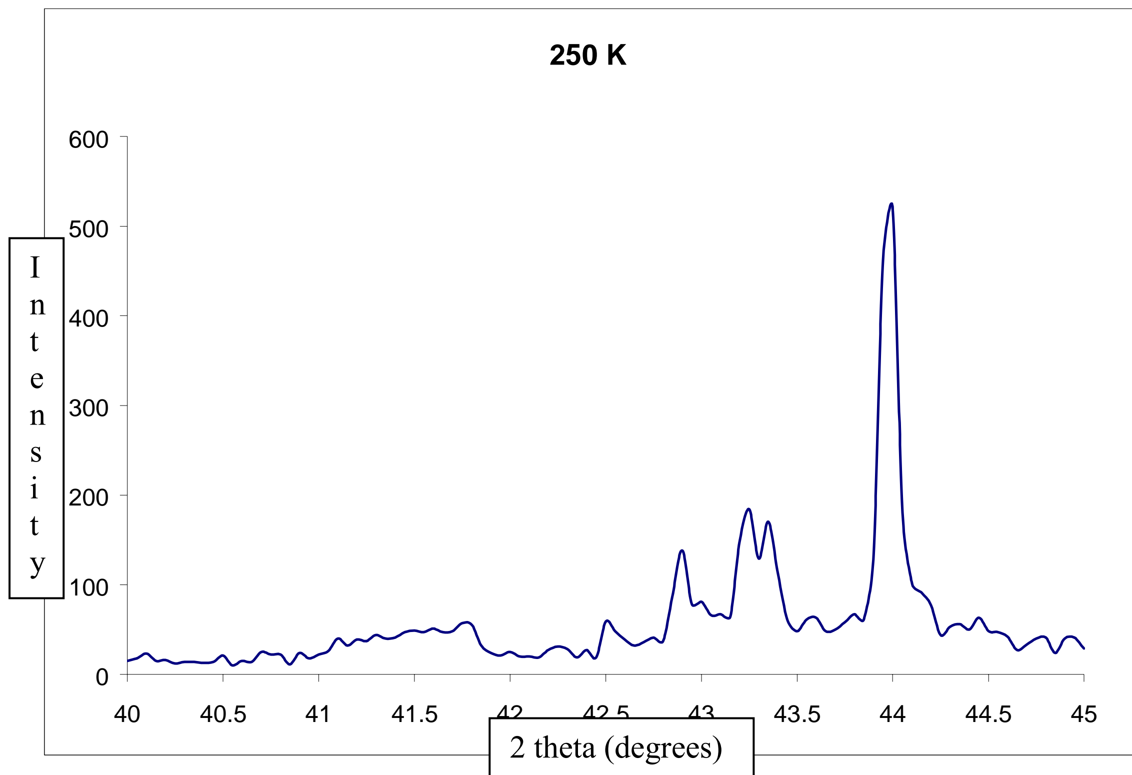

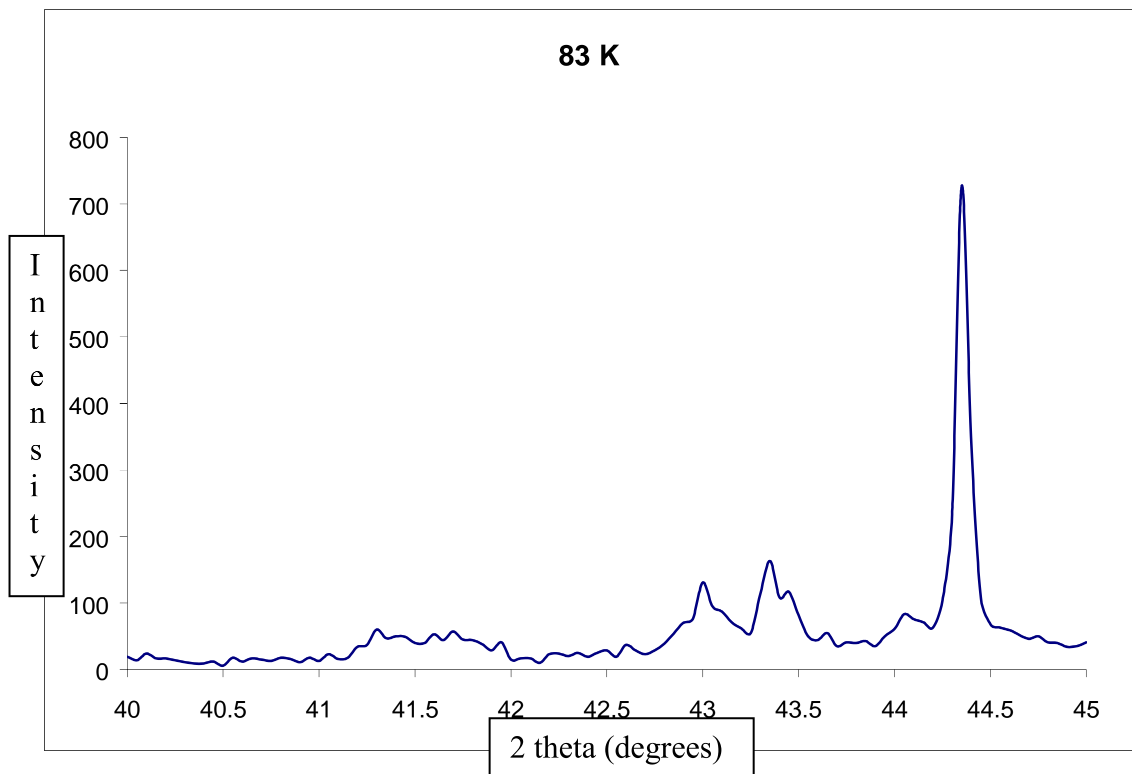

Fig. 3.15: Fragments of diffraction patterns of the $TlInS_2$ crystal at two sample temperatures T, 250, and 83 K, from top to down.

3.5 Results of DSC Measurements

This section deals with the specific heat capacities of $TlInS_2$ and $TlGaS_2$ crystals obtained by Differential Scanning Calorimetry (DSC) method at low temperatures. For these measurements, we used DSC 2010 equipment from TA Company instruments. DSC 2010 is advanced equipment providing a fundamentally more accurate way of measuring heat flow. It supplies information for the direct measurement of the heat capacity. DSC 2010 has the reference and sample cells made of platinum-iridium alloy. These cells with a thermometer and a heater are mounted in an aluminum heat sink kept nearly at the temperature of the cooling bath. The heat sink is cooled with liquid nitrogen. The level of liquid nitrogen is kept constant during the DSC measurements. In order to purge the system, helium gas is constantly passed through the heat sink and over the cells. The sample and reference pans are covered with an aluminum foil. Pan and the covers are folded up with a special tool. In this mechanism, the folded up sample pan is placed in one cell, and the folded up empty pan is placed in the other cell. After calibration for temperatures and calorimetric sensitivity of the DSC equipment, the optimum heating rate was determined to be 10 K per min. The raw DSC curves of $TlInS_2$, $TlGaS_2$ and baseline are shown in Fig.3.16 in the temperature range 140 to 300 K.

In the calculation process, we have used a formula suitable for calculating heat capacity using the data of our apparatus

$$C_p = \left(\frac{60.E}{Hr}\right)\frac{\Delta H}{m} \tag{3.5}$$

where

ΔH: the difference heat flow of the sample and empty pan at the same rate.

Hr: heating rate

E: cell calibration constant

m: mass of the sample

For the value of E = 1.0768 which is given by our system and the masses of $TlInS_2$ and $TlGaS_2$ as 14.5 mg and 8.5 mg, respectively, we have calculated the heat capacities of the two samples for different temperature values. The heat capacities for each temperature value are converted to J/ (mol. K) and tabulated in Table 3.2.

The heat capacities versus temperature graphs were plotted for both crystals. Fig. 3.17 and 3.18 show temperature dependences of the specific heat capacities of TlGaS2 and TlInS2 single crystals, respectively. The data obtained for the temperature variation of the specific heat capacity for $TlGaS_2$ and $TlInS_2$ were compared with the available data in the literature.

Specific heat capacities of TlGaS2 were calculated from DSC data obtained in the temperature range of 170-240 K. Fig. 3.17 shows the temperature dependence of heat capacity for $TlGaS_2$. The heat capacity of $TlGaS_2$ rapidly decreases in 170-185 K range and stays almost stable in 185-200 K. Then the data show continous increase from about 83 J/ (mol. K) to 105 J/ (mol. K) in 210-240 K. We could find only one published information related to the specific heat capacity measurement of $TlGaS_2$. Krupnikov and Abutalybov [60] investigated the temperature-dependent of specific heat capacity of pure and doped single crystals of $TlGaS_2$ in temperature range of 60-280 K. The heat capacity data of $TlGaS_2$ presented by Krupnikov et al. [60] agree well with our data. But they reported an anamolues increase and decrease of C_p around 187 K that we did not observe. They interpreted this anomaly to be

related to phase transition at this temperature.

Fig. 3.18 shows the temperature dependence of heat capacity of $TlInS_2$ that we have obtained from the DSC data. The heat capacity of $TlInS_2$ decreases rather rapidly with temperature from 170 K up to about 200 K. Then, the graph shows decrease with temperature at a slower rate. The data demonstrate some small fluctuations. There are only two reports in the literature about the heat capacity of $TlInS_2$. There are reasonable agreements about the temperature dependence of our data and those of the references [23, 24]. Aldzhanow et al. [23] determined one of them. C_p values and that reported in Ref. [23] fluctuate between 185 and 230 K, but the degree of fluctuation is high in Ref. [23]. The authors of Ref. [24] revealed additional anomalues variations of C_p (T) in the range 196.9-214.9 K that we did not observe.

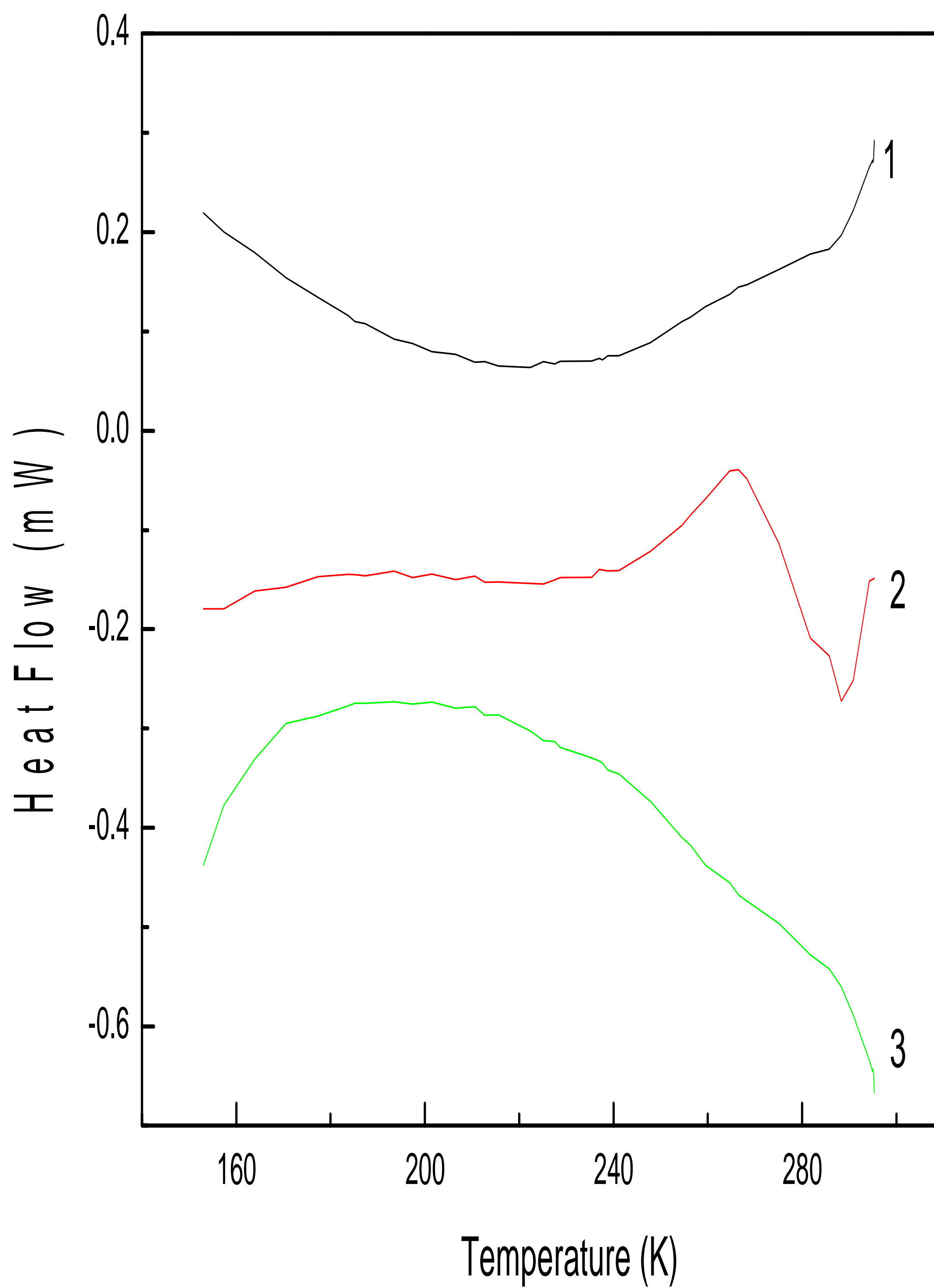

Fig. 3.16: DSC curves of 1-baseline, 2-$TlInS_2$, and 3-$TlGaS_2$

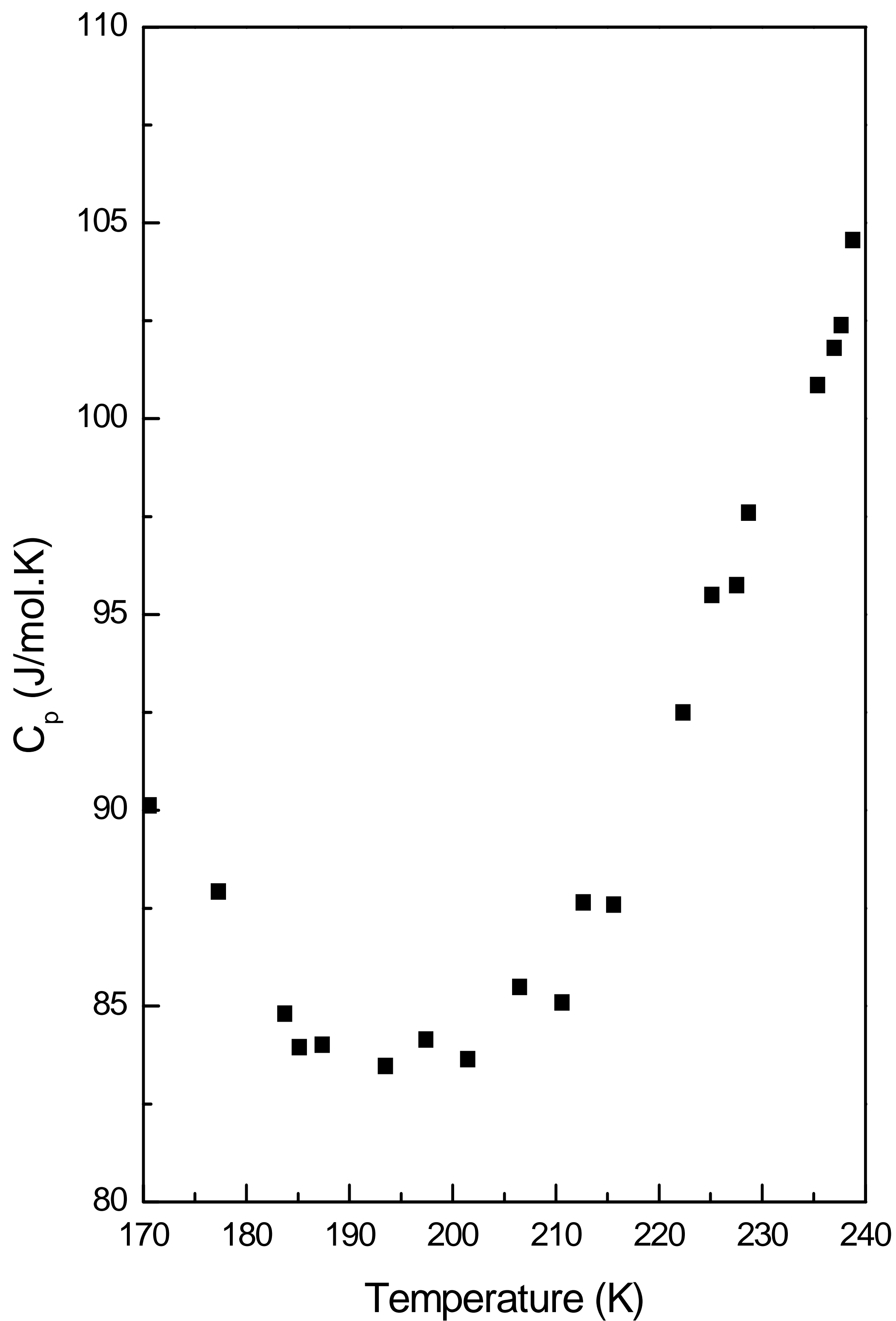

Fig. 3.17: Temperature dependence of the specific heat of TlGaS2 single crystal determined in the range 170-240 K.

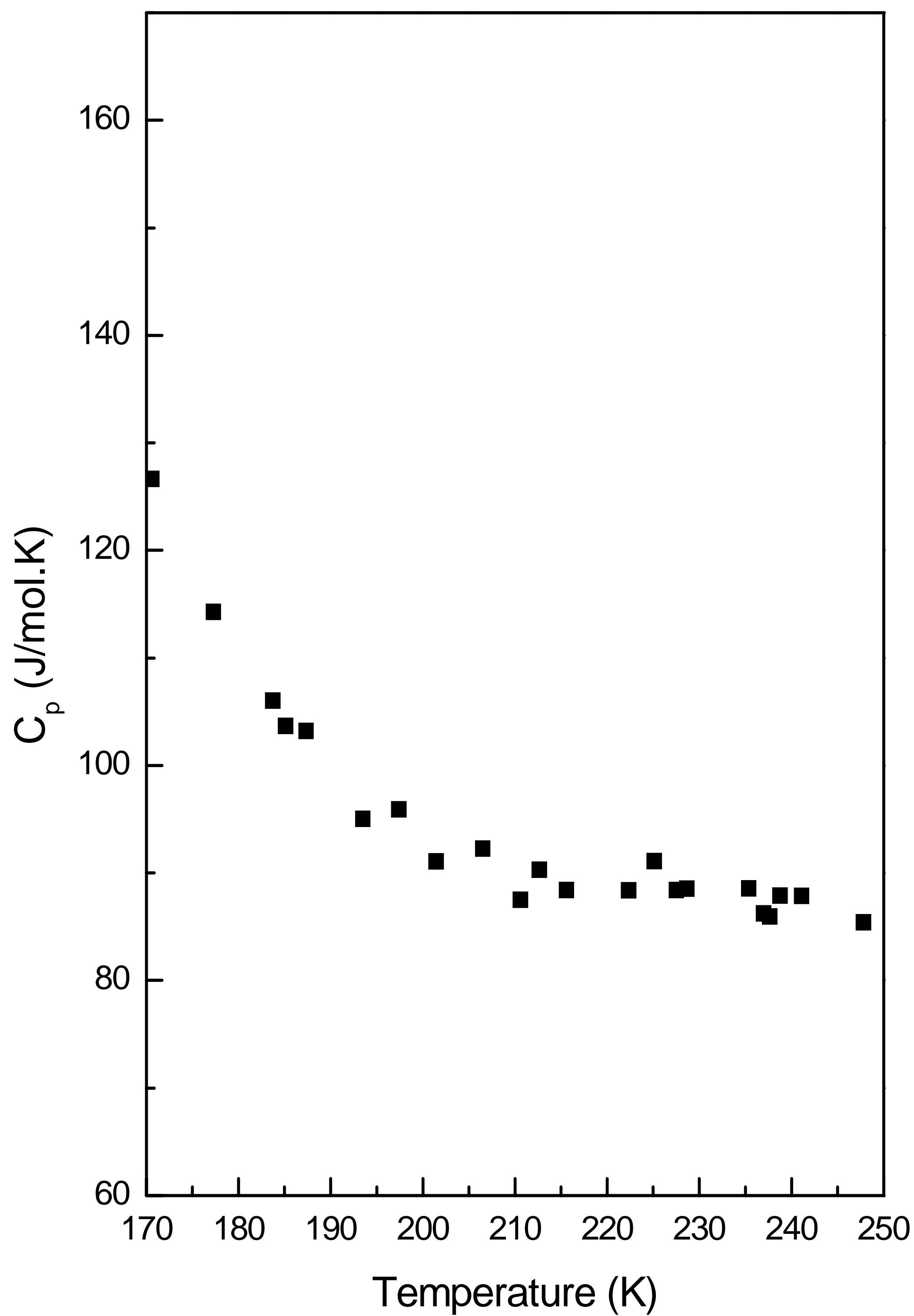

Fig. 3.18: Temperature dependence of the specific heat of $TlInS_2$ single crystal determined in the range 170-250 K.

Table 3.2: Calculated heat capacities of $TlInS_2$ and $TlGaS_2$ at various temperatures

$TlInS_2$		$TlGaS_2$	
T, K	C_p, J/K.mol	T, K	C_p, J/K.mol
170.59	126.63923	170.59	89.59988
177.28	114.28418	177.28	87.41081
183.72	106.03393	183.72	84.30963
185.13	103.67672	185.13	83.45832
187.34	103.18902	187.34	83.51913
193.49	95.03225	193.49	82.98098
197.4	95.88979	197.4	83.65291
201.46	91.07376	201.46	83.15124
206.5	92.27269	206.5	84.99067
210.6	87.51356	210.6	84.59238
212.66	90.30157	212.66	87.13414
215.61	88.39548	215.61	87.07637
222.33	88.37516	222.33	91.95617
225.12	91.09815	225.12	94.93574
227.53	88.38735	227.53	95.18809
228.67	88.52553	228.67	97.02448
235.38	88.54992	235.38	100.26552
236.98	86.23741	236.98	101.21108
237.65	85.94886	237.65	101.78571
238.78	87.90372	238.78	103.94742
241.11	87.84275	241.11	105.14836

CHAPTER 4

CONCLUSION

A wide variety of ternary layered semiconductors receives much attention due to their optical and electrical features as possible light emitters in optoelectronic device applications from ultraviolet to infrared. The presence of three different chemical compounds allows the gathering of several significant properties. Therefore, the physicochemical properties of ternary compounds also have attracted a valuable attention in addition to fundamental and technological interest. In view of its possible applications in optoelectronic devices, a great deal attention has been devoted to the study of the optical and electrical properties of $TlGaS_2$. In this concern, detailed information about the properties of $TlGaS_2$ is very useful for the fabrication of high quality devices.

In the photoluminescence part of this work, we report the results of the PL investigation of $TlGaS_2$ single crystals in the 500-1400 nm wavelength and in the 15-115 K temperature range. From the laser excitation intensity dependence and temperature dependence of PL spectra, we obtained the following results for $TlGaS_2$.

We observed three broad bands with an asymmetric Gaussian line shapes centered at 568 nm (2.183 eV, A-Band), 718 nm (1.727 eV, B-Band), and 1102 nm (1.125 eV, C-Band) in the PL spectrum. The emission band intensity, half width, and peak position changed with respect to temperature. These features are typical of emission bands, which are due to donor-acceptor pair transitions observed in ternary semiconductors. The A- and B- bands were found to be due to radiative transitions from the deep donor levels located at 0.362 eV (d_1) and 0.738 eV (d_2) below the

bottom of the conduction band to the shallow acceptors levels at 0.005 eV (a_1) and 0.085 eV (a_2) located above the top of the valence band, respectively. The presence of these two acceptor levels explains the thermal quenching behavior of the A- and B- bands in PL spectra of $TlGaS_2$ crystal.

The peak energy of C-band does not change with increasing excitation laser intensity. This result rules out the model of distant donor-acceptor pair (DAP) recombination process where a shift toward higher energies are expected as the excitation laser intensity is increased. In terms of the CC model, the observed quenching of the C-band in the PL spectra with increasing temperature is due to an increased electron population of the excited state at higher displacement coordinates.

Indexing studies and analysis using powder x-ray diffraction data showed that $TlInS_2$ has hexagonal system with lattice parameters a = 3.83 and c = 14.88 A^o. $TlGaS_2$ has monoclinic system with lattice parameters a = 9.62, b = 4.01, c = 7.52 A^o and $\beta = 96.30^o$. Diffraction measurements on our samples at low temperatures do not show evidences for the occurrence of incommensurate phase transition in the range of 200-214 K as pointed out by Sheleg et al. We propose that the growth conditions and the amounts of impurities may be effective for the phase transitions of these crystals at low temperatures.

Finally, specific heat capacity measurements have been carried out for $TlInS_2$ and $TlGaS_2$ using Differential Scanning Calorimetry (DSC) method. Specific heat capacities of these crystals have not been investigated by DSC method before. The C_p (T) data obtained for $TlGaS_2$ and $TlInS_2$ agree reasonably well with the available data in the literature with some deviations at low temperatures. The results of these measurements showed that we can use DSC method to determine the specific heat capacities of chalcogenides.

REFERENCES

[1] L. I. Berger, *Semiconductor Materials*, CRC Press, Boca Raton, 1997.

[2] G. G. Stokes, *Philos. Trans. R.*, Soc. London A 142:463, 1852.

[3] Klaus D. Mielenz,
Optical radiation measurements: Measurement of Photoluminescence,
p. iv, Academic Press, New York, 1982

[4] R. A. Stradling and P. C. Klippstein, *Linhtowlers in Growth and Characterization of Semiconductors*, Bristol, 1990.

[5] C. B. Collins, R. D. Carlson and C. J. Gallagher, *Phys. Rev.*, 105:1168, 1957.

[6] K. A. Yee and A. Albright, *J. Am. Chem. Soc.,* 113:6474, 1991.

[7] A. G. Kyazmazade, R. N. Mekhtieva, and A. A. Akhmedov, *Sov. Phys. Semocond.*, 25:840, 1992.

[8] S. K. Deb and A. Zunger (Ed), *Proc. 7th Internat. Conf. Ternary and Multinary Compounds*, MRS, Pittsburgh, 1987.

[9] S. I. Radautsan and Schwab (Ed), *Proc. 7th Internat. Conf. Ternary and Multinary Compounds*, Stiintsa Press, Kishinev, 1992.

[10] D. Muller and H. Z. Hahn, *Anorg. Allg. Chem.*, 438:258, 1978.

[11] N. M. Gasanly et al., *Solid State Commun.*, 105:21, 1998.

[12] M. P. Hanias, A. N. Anagnostopoulos, K. Kambas, and J. Spvridelis, *Mat. Res. Bull.*, 27:25, 1992.

[13] N. Kalkan, J. A. Kalomiros, M. Hanias, and A. N. Anagnostopoulos, *Solid State Commun.*, 99:375, 1996.

[14] B. Abay, H. S. Guder, H. Efeoglu, and Y. K. Yogurtcu, *Solid State Solidi (b)*, 227:469, 2001.

[15] K. Allakhverdiev, T. G. Mammedov, R. Suleymanov, and N. Z. Gasanov, *J.Phys.: Condens. Matter*, 15:1291, 2003.

[16] H. J. Song, S. H. Yun, and W. T. Kim, *Solid State Commun.*, 94:225, 1995.

[17] A. Kato, M. Nishigaki, N. Mammedov, M. Yamazaki, S. Abdullayeva, E.

Kerimova, H. Uchiki, and S. Lida, *J. Phys. Chem. Sol.*, 64:1713, 2003.

[18] N. S. Yuksek, N. M. Gasanly, and H. Ozkan, *Semicond. Sci. Techol.*, 18:834, 2003.

[19] N. M. Gasanly, A. F. Goncharov, N. N. Melnik, A. S. Ragimov, and V. I. Tagirov, *Phys. Stat. Solidi*. (b), 116:427, 1983.

[20] G. I. Abutalybov and E. Yu. Salaev, *Sov. Phys. Solid State*, 28:1231, 1986.

[21] S. G. Abdullaeva, N. T. Mamedov, F. A. Mustafaev, and E.Yu. Salaev, *Phys Status Solidi.* (a), 82:K75, 1984.

[22] H. Hahn, B. Wellmann, *Naturwissenschaften*, 54:42, 1967.

[23] M. A. Aldzhanov, N. G. Guseinov, and Z. N. Mamedov, *Sov. Phys. Solid State*, 30:580, 1987.

[24] K. K. Mamedov, A. M. Abdullaev, and E. M. Kerimova, *Phys. Stat. Sol. (a),* 94:115, 1986.

[25] S. G. Abdullaeva, A. M. Abdullaev, K. K. Mamedov, and N. T. Mamedov, *Sov. Phys. Solid State*, 26:618, 1984.

[26] S. Wang, *Fundamentals of Semiconductor Theory and Device Physics*, Prentice Hall, New Jersey, 1989.

[27] E. S. Yang, *Fundamentals of Semiconductor Devices*, Mc Graw-Hill, New York, 1988.

[28] Yu. P. Gnatenko, I. A. Farina, R. V. Gamernik, V. S. Blashkiv, and A. S. Krochuk, *Semiconductors*, 30:1027, 1996.

[29] J. I. Pankove, *Optical Processes in Semiconductors*, p. 150, Prentice Hall, New Jersey, 1971.

[30] R. B. Adler, *Introduction to Semiconductor Physics*, Wiley, New York, 1964.

[31] K. Seeger, *Semiconductor Physics*, Springer-Verlag, New York, 1973.

[32] B. Hendersen, *Defects in Crystalline Solids*, Crane, Russak, New York, 1972.

[33] P. Y.Yu., M. Cardona, *Fundamentals of Semiconductors*, p. 344, Springer, Berlin, 1995.

[34] B. Hendersen and A. E. Hughes, *Defects and Their Structure in Nonmetallic Solids*, Plenum Press, New York, 1976.

[35] H. W. Leverenz, An Introduction to Luminescence of Solids, RCA Laboratories Princeton, N. J., 1968.

[36] Klaus D. Mielenz, *Optical radiation measurements: Measurement of Photoluminescence*, p. iv, Academic Press, New York, 1982.

[37] T. Schmidth, K. Lischka, and W. Zulehner, *Phys. Rev.*, B45:8989, 1992.

[38] P. J. Dean, Prog. Cryst. Growth Charact. 5:89, 1982.

[39] T. Taguchi, J. Shirafuji and Y. Inuishi, *Phys. Status Solidi B* 68:727, 1975.

[40] D. E. Cooper, J. Bajaj and P. R. Newmann, *J. Cryst. Growth,* 86:544, 1988.

[41] Z. C. Feng, A. Mascarenhas and W. J. Choyke, *J. Lumin.* 35:329, 1986.

[42] Q. Kim and D. W. Langer, *Phys. Status Solidi B,* 122, 263, 1984.

[43] A. G. Milnes, *Deep Impurities in Semiconductors*, p. vii, John Wiley and Sons, New York, 1973.

[44] E. W. Nuffield, *X-ray Diffraction Methods*, John Wiley & Sons, Inc., 1966.

[45] B. D. Cullity, *Elements of X-ray Diffraction*, Addison-Wesley Publishing Company, Inc., 1967.

[46] H.G. Kim, K. H. Park, B.N. Park, H.J. Lim, S. K. Min, H. L. Park and W. T. Kim, *Jap. J. Appl. Phys.,* Suppl. No. 3, 32:476, 1993.

[47] N. M. Gasanly, A. Aydinli, A. Bek, and I. Yilmaz, *Solid State Commun.*, 105:21, 1998.

[48] J. Krustok, H. Collan , and K. Hjelt, *J. Appl. Phys.* 81**:**1442, 1997.

[49] T. Schmidt, K. Lischka, and W. Zulehner, *Phys. Rev.,* B 45**:**8989, 1992.

[50] P.Y. Yu and M. Cardona, *Fundamentals of Semiconductors*, Springer, Berlin, 1995, p. 348.

[51] J. Krustok, J.H. Schon, H. Collan, M. Yakushev, J. Mudasson, and E. Bucher, *J. Appl. Phys.*, 86:364 1999.

[52] C. J. Hwang, *Phys. Rev.*, 180:827, 1969.

[53] S. Shigetomi, T. Ikari, and H. Nakashima, *J. Appl. Phys.*, 74:4125, 1993.

[54] R. K. Willardson, and A. C. Beer, *Semiconductors and Semimetals,* Academic Press, New York, vol. 8, 1972, p.374.

[55] J. I. Pankove, *Optical Processes in Semiconductors*, p. 150, Prentice Hall, New Jersey, 1971, p.150.

[56] V. Capozzi, *Phys. Rev.*, B28:46, 1983.

[57] A. U. Sheleg, O. B. Plynshch, and V. A. Aliev, *Sov. Phys. Solid State*, 36:226, 1994.

[58] M. P. Hanias, A. N. Anagnostopoulos, K. Kambas, and J. Spyridelis, *Mat. Res.Bull.*, 27:25, 1992.

[59] N. M. Gasanly, A. F. Goncharov, N. N. Melnik, A. S. Ragimov, and V. I. Tagirov, *Phys. Stat. Solidi (b)* , 116:427, 1983.

[60] E. S. Kuripnikov and G. I. Abutalybov, *Sov. Phys. Solid State*, 34:702, 1992.